RADICAL PROBE SYSTEM FOR IN-SITU MEASUREMENTS OF RADICAL DENSITIES OF HYDROGEN, OXYGEN AND NITROGEN

BY

DREN QERIMI

THESIS

Submitted in partial fulfillment of the requirements
for the degree of Master of Science in Nuclear, Plasma, and Radiological Engineering
in the Graduate College of the
University of Illinois at Urbana-Champaign, 2019

Urbana, Illinois

Master's Committee

Professor David N. Ruzic, Advisor

Assistant Research Professor Daniel Andruczyk

Abstract

The current state-of-the-art methods to identify presence of radical species in vacuum chambers are optical methods, which suffer from the lack of spatial resolution and require expensive optical equipment. In this study Center for Plasma Material Interactions (CPMI) at the University of Illinois developed an in-situ catalytic radical probe system together with Ra-Den software platform to measure concentrations of reactive species in low temperature plasma with high spatial resolution. Radical probes as plasma diagnostic tool can be used to determine radical densities of hydrogen, nitrogen and oxygen but not limited to in any continuous plasma source in vacuum environment. The basic principle and advantage of a probe array is the capability to distinguish between different gas species due to several sensitive elements acting as recombination catalysts [1] [2]. The catalytic coatings cover an area of several square millimeters on the tip of a sheathed thermocouple. The catalytic probe surface provides efficient recombination of active species with subsequent energy release as a heat. All the probes are exposed to the same background plasma heating/cooling mechanisms, but the temperatures are not the same due to the fact that different catalytic materials have different recombination coefficients, therefore a temperature difference between probes is generated. The system consists of two additional probes, first to obtain the overall heat flux on probe array, and the second is a reference probe with surface chemically active to all gases. Radical densities of hydrogen, nitrogen and oxygen were measured in HARP helicon chamber by sweeping power from 300W up to 1100W and by sweeping pressure from 10mT up to 100mT. Generally, it is observed that radical densities increase with respect to pressure and power, accordingly. Additionally, plasma is parametrized by electron density and elec-

tron temperature such that electron density increased with increasing power and pressure and electron temperature increased with increasing power but it did decrease with increasing pressure. Further tests showed that radical probe system is capable is detecting specific gases when a mixture of gases is present in the chamber based on known recombination coefficient of the given gas on catalytic surface. Ionization and radical density percentages of all three gases are compared to total ionization cross-sections of each gas, agreement is observed for each corresponding gas. The array of several probes is capable to distinguish between different gas species with sub centimeter spatial resolution. The probes give accurate results in a broad range of reactive species concentrations from about $10^{12}\ cm^{-3}$ to $10^{14}\ cm^{-3}$.

Acknowledgments

I am humbly thankful to God for blessing me and giving me everything and I thank my family for unconditional love and support in every single step of my life since my childhood back in Kosovo. I would like to thank my parents, Bujar and Mirvete Qerimi, for their sacrifice in order to educate my siblings and I. A thank you from the bottom of my heart is for my dear mother who is such an astounding woman with remarkable personality and who's support for my family will be eternally appreciated. Very special thank you to my dear wife Hadil Kibech, who's love and patience has been an solid anchor of support and motivation for me, without which I would have not been able to succeed.

I would like to thank my advisor, professor David Ruzic for trusting me and giving me the opportunity to be part of his research group when I started as an undergraduate assistant. His guidance and support is what made my academic dream come true, you are a person in which I find motivation, hope and a great role model. Without your genuine advises and support, my path that I chose would have been impossible. Your impact on my work ethic and education is to never be forgotten.

My journey would have very difficult without friends and colleagues which I have made at CPMI, I would like to thank everyone for their friendship, their willingness to share wisdom, for being great friends which make life on day to day basis very pleasant. Special thanks go my initial mentors Ivan Shchelkanov, Wenyu Xu, Roland Wu, Peter Fiflis and Priya Raman, for the guidiance and for sharing their vast knowledge. Also I would like to thank from my heart Gianluca Panici, Pawel Piotrowich, Michael Christianson, Matthew Szot, Aveek Kapat, Jan Uhlig, Stephen Stemmly, Dhruval Patel and Tag Choi. It is a great honor to

learn from you. Also, I would like to thank my undergraduate assistant for doing all the hard work, James Wagner, Andreas Calliagaris, Alyssa Hayes, Brandon Pelc, Ari Jain, Sowmya Panuganti, Daniel Jacobson and Brian Park. I would like to thank Brian Jurzyck, Robert Stubbers and Starfire Industries for their technical support and advice.

Table of Contents

List of Tables

List of Figures

Chapter 1

Introduction

1.1 Motivation

Free radicals play a very important role in many chemical reactions due to their high reactivity towards other molecules and toward themselves. Need to quantify the presence of radicals has increased in industry in the recent years. Currently, the state-of-the-art methods to determine radical presence and their density inside vacuum chambers is via optical emission spectroscopy (OES) which is expensive method and lacks spatial resolution. Center for Plasma Material Interactions (CPMI) at the University of Illinois developed a probe system array (catalytic probe) to measure in-situ concentration of reactive gas spices in low temperature plasma with high spatial resolution. Radical probes as plasma diagnostic tool can be used to determine radical densities of hydrogen, nitrogen and oxygen in any continuous plasma source in vacuum environment. Radical probe are also capable of in-situ measuring all the above mentioned gases simultaneously as well as independent species. Degradation of the radical probes occur over time via oxidation of probes or catalytic material can etch away. However, removing oxide layers can be achieved via in-situ sputtering of the probes and reapplying catalytic material is a fairly simple deposition process, it is inexpensive. This study shows measurements of radical densities with respect to pressure and power in a helicon plasma source as well as measurements of plasma parameters such as electron density and electron temperature.

1.2 Thesis Statement

The purpose of this work is to design and build a radical probe system which is simpler and cheaper than optical methods. Radical probe system can measure radical densities of hydrogen, oxygen and nitrogen in continuous plasma environment and it can be used in various industrial and research applications. System of radical probes include its own developed software which allows for in-situ measurement of radical densities. This system has the capability to be expanded to measure numerous radical densities of different gases when proper pair of catalytic coating and gas is combined.

1.3 Previous Work

Need to detect and understand radical densities has generated numerous measurement techniques which are depend on nature of plasma environment and on the need of invasiveness. Such technique is laser-induced fluorescence (LIF) which is sensitive method to detect atoms, radicals and ions by measuring species concentration and energy-level population distributions by exciting particles from ground electronic levels to an exited state via laser radiation, thus, absorbing laser photon. Then excited species de-excite by emitting a fluorescence photons [12]. Only a fraction of excited species emit fluorescence photons, thus, an optical filter is used to res-shift fluorescence light at a certain emission wavelength which are detected by the camera. LIF is used mostly for in fluid mechanical processes such as plasma jets with high spatial and temporal resolution. *Yonemori et al.* [3] uses LIF method to determine oxygen radical density due to oxygen chemical reactiveness from an atmospheric-pressure helium plasma jet which serves as cancer treatment biomedical device. **Figure 1.1b** shows time evolution of oxygen density radial distribution on a skin sample.

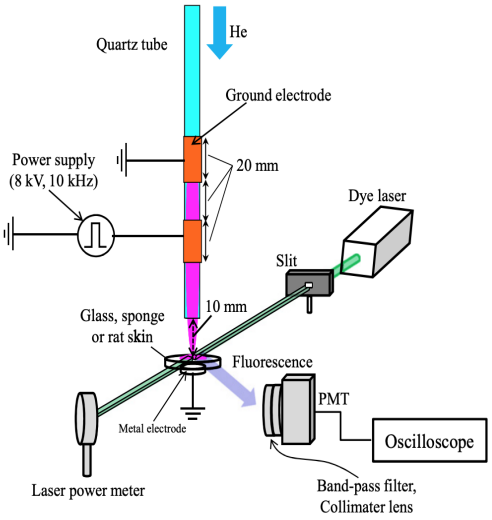

(a) Schematic diagram of LIF system.

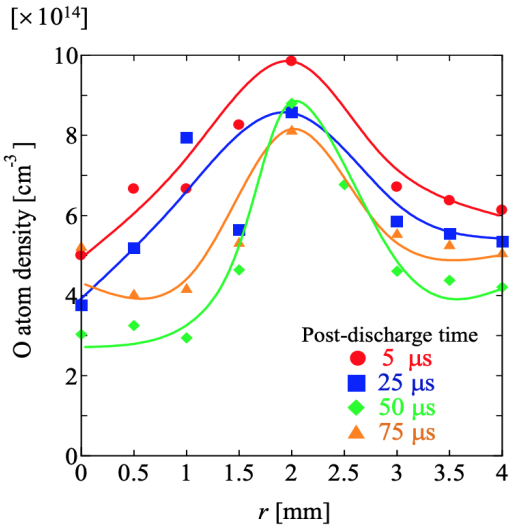

(b) Time evolution of O atom density radial distribution

Figure 1.1: Flux of O radicals onto a surface by an atmospheric-pressure helium plasma jet measured by laser-induced fluorescence by *Yonemori et al* [3].

Another radical density spectroscopy measuring technique is two-photon laser-induced fluorescence (TALIF). TALIF operating principle is similar to LIF, however, TALIF uses two photons to excite an atom instead of one [13]. Such it is possible to use two photons of different wavelengths in order to achieve excitation of species which brings many advantages as seen in [14]. *Mazouffre et al.* [4] reported local macroscopic properties of ground-state nitrogen atoms by TALIF spectroscopy, where nitrogen atoms at excited via two 206.7 nm photons from $2p^4S_{3/2}$ ground state to the $3p^4S_{3/2}$ state in a nitrogen plasma jet. The excited fluorescence state emission was collected by a gated photomultiplier tube (Hamamatsu R928), see **figure 1.2**. Density of ground-state nitrogen atoms profile is shown in **figure 1.3**. TALIF spectroscopy similarly with LIF can use utilized for measurements of varieties of species.

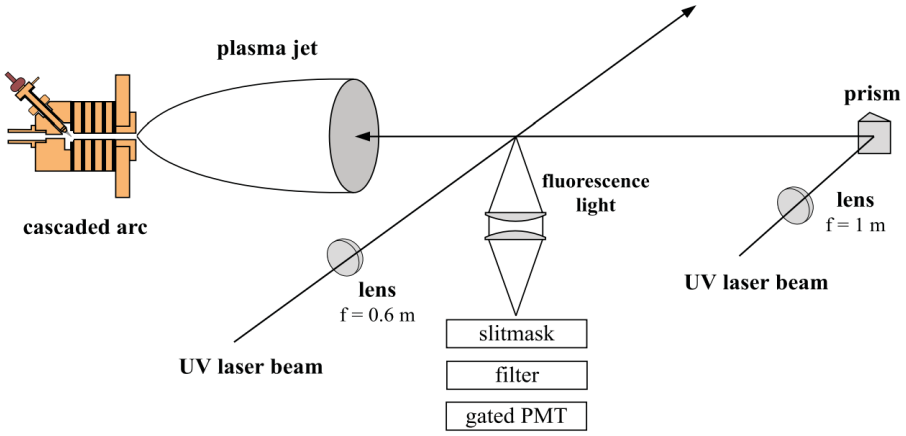

Figure 1.2: Schematic view of the experimental arrangement used to spatially probe ground-state nitrogen atoms by means of TALIF spectroscopy [4].

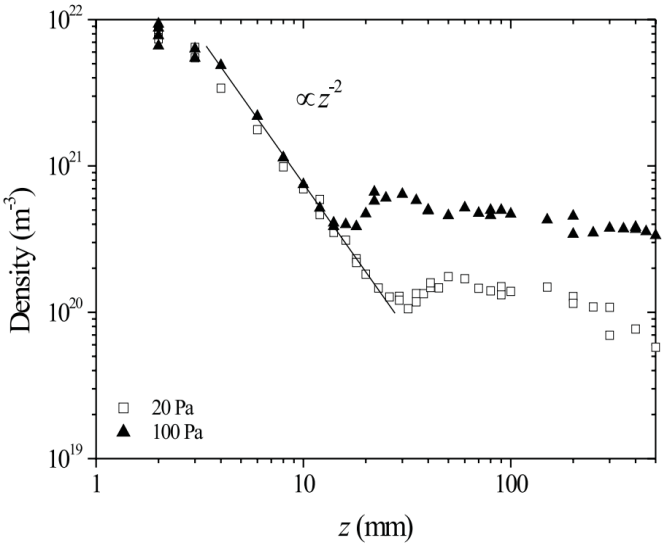

Figure 1.3: Ground-state nitrogen atom density profile along the jet centreline at 20 Pa and 100 Pa background pressure [4].

.

Additionally, Auger electron spectroscopy (AES) has been used to determine radical density as well as surface recombination of radicals. Operating principle of AES relies by exciting species on the surface via focused electron beam which causes Auger electron to be emitted as consequence [15]. *Guha et al.*[5] reports in-situ measurements of oxygen recombinations on heavily oxidized surfaces by observing chemical composition of the surface

and time-dependent changes in oxygen radical coverage via AES during plasma operation at different plasma frequencies. **Figure 1.4** shows recombination oxygen coefficient as function of oxygen plasma flux.

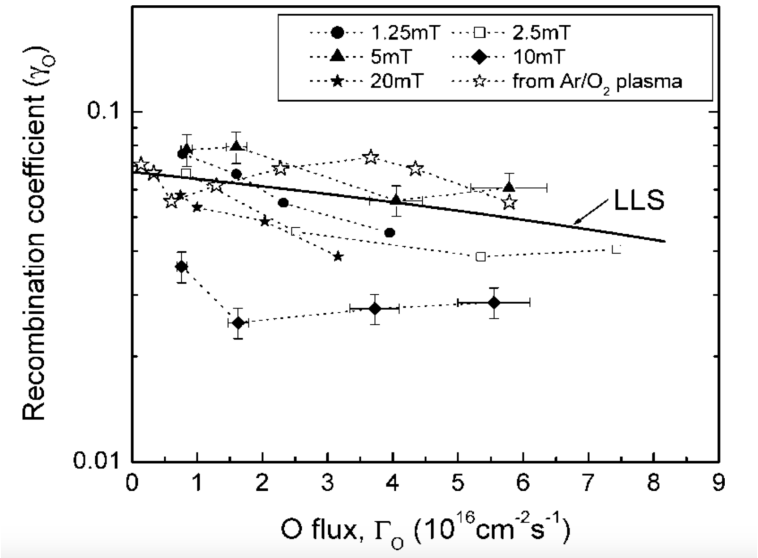

Figure 1.4: Recombination coefficient (γ_O) on an anodized aluminum surface as a function of O flux (Γ_O) in the plasma. The line labeled LLS is a linear least-squares fit to all the values [5].

This study was based on the work of *Mozetic et. al.*[1][2][6][16][17][18] where two catalytic probes are utilized to determine a given radical density by the following fashion. Two radical probes with different catalytic surfaces are installed inside the vacuum chamber system containing desired plasma gas. Density of random flow on the probe surface per unit time is given as:

$$j = \frac{1}{4} n \langle v \rangle \tag{1.1}$$

where n is the atomic density of the gas near the probes and $\langle v \rangle$ is mean velocity. Energy absorbed by probe surface per unit time is given as probe heating mechanism:

$$P_h = \frac{1}{2} j \gamma W_D A_p \tag{1.2}$$

where γ is surface recombination coefficient, W_D is the dissociation energy of a hydrogen molecule dissipated at the surface as the recombination takes place and A_p is surface area of the probe. During operation, probe temperature is higher then gas temperature due to energy absorbed by the probes due to recombinations of radicals. The density is calculated when the flow of atoms is interrupted for a certain time interval or plasma is shut off such that temperature of the probes decrease with time. First derivative with respect to time of the probe temperature $T = T(t)$ is measure of the cooling mechanism.

$$P_c = MC_p \frac{dT}{dt} \tag{1.3}$$

where M is the mass of the catalytic material on the probe tip and C_p is specific heat capacity of the catalytic material. Thus by equating 1.2 and 1.3:

$$n = \frac{4MC_p(\frac{dT}{dt})}{\sqrt{\frac{8k_BT}{\pi m}}\gamma W_D A_p} \tag{1.4}$$

Equation 1.4 calculates radical density in the vicinity of the probe. This method is very similar to method used in this study however the difference is based on the operating regime. *Mozetic et al.*[1] method calculates radical density in the moment when either gas flow is stopped or plasma is shut off, shown in **figure 1.5b**. Similarly, *Sorli et al* [19] shows radical densities using the same method, see **figure 1.5a**. However, our method determines radical density in-situ in steady state condition, also, it is capable of detecting and measuring radical densities of three gases simultaneously due to its design which includes an array of probes.

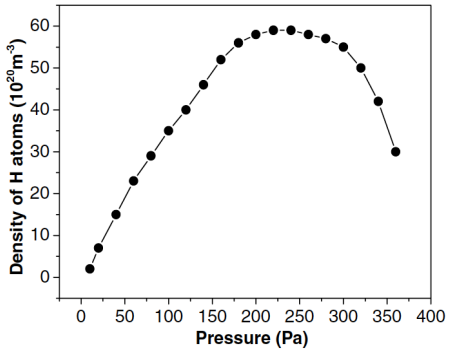

(a) Density of neutral hydrogen atoms in the afterglow of RF plasma [2].

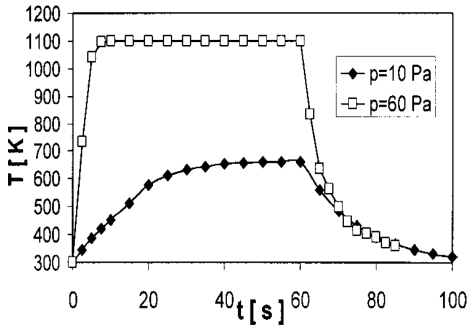

(b) Temperature of the catalytic probe during exposure to hydrogen atoms at two different pressures [19].

Figure 1.5: Density of H atom based on temperature decay by *Mozetic et al.*[1]

Chapter 2

Theory

2.1 Radical Probe Theory

The most important parameter in low temperature reactive plasmas is often the density of neutral atoms due to information they give for any given processing technique. The probes take advantage of catalytic heterogeneous surface recombination of neutral atoms. Due to high recombination coefficients of the catalytic surface of the probe, the probes are heated to a high temperature during exposure to highly dissociated gas such as reactive plasma. The catalyst temperature depends on the flux of neutral atoms on the probe tip. In order to prevent a substantial drain of atoms by the probe, probe size should be designed as small as possible. A typical dimension of a modern catalytic probe is 1 mm or less. The principle of the probe operation is extremely simple: when a piece of metal is exposed to atmosphere rich of neutral active atoms, the metal surface is exposed to a large flux of the atoms. The atoms tend to recombine on the surface, thus causing heating of the metal. The amount of heat released on the metal surface depends on the flux of radicals and recombination efficiency of this particular metal surface. The flux of atoms onto the catalyst surface can be recalculated from measured amount of heat by using an appropriate physical model. Each probe system consists of two probes: one which has catalytic material coated on the tip via magnetron sputtering and another probe which is bare stainless-steel. When exposed in the same plasma environment and in the same physical space, probes read two different temperatures due to temperature dependence of recombination coefficient in each probe. This temperature difference is proportional to radical density in the space near the probes.

Catalytic probes can be in a variety of configurations. Basically, there are two options: either to measure the catalyst temperature, or keep the temperature constant by external heating and measure the power supplied to sustain a constant temperature. Both options have advantages and disadvantages. The first option is sensitive to possible variations of the recombination coefficient with temperature. The second one is not sensitive to the variations of recombination coefficient, because temperature is kept constant, but the size of the probe is much bigger, and it may disturb plasma [20]. The three most commonly used designs of catalytic probes are shown in **figure 2.1**.

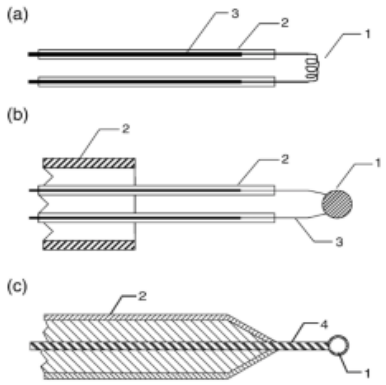

Figure 2.1: Most commonly used catalytic probes: a probe with external heating, a simple thermocouple probe without external heating, a fiber optics catalytic probe; 1 catalyst, 2 probe holder, 3 thermocouple wires, 4 optical fiber [6].

The radical density in the vicinity of the probe is calculated as follows:

$$\frac{nW_D v A \gamma_{probeA}}{8} = P_{thermal\,conduction} + P_{thermal\,emission} \tag{2.1}$$

Where, thermal conductivity and thermal emission are:

$$P_{thermal\,conductivity} = \frac{\chi S \Delta T}{l} \tag{2.2}$$

$$P_{thermal\,emission} = \varepsilon \sigma T^4 S \tag{2.3}$$

Here, n is radical density, W_D is the dissociation energy from the parent molecule, v is velocity of radicals, A surface area of catalytic material, γ is recombination coefficient of radicals on catalytic surface, χ is thermal conductivity of steel, S is the cross-sectional area of the probe, T is the temperature, l is the length of the probe, ε is the emissivity factor and σ is the constant of proportionality or Stefan-Boltzmann constant. **Figure 2.2** shows schematics of working principle of radical probes.

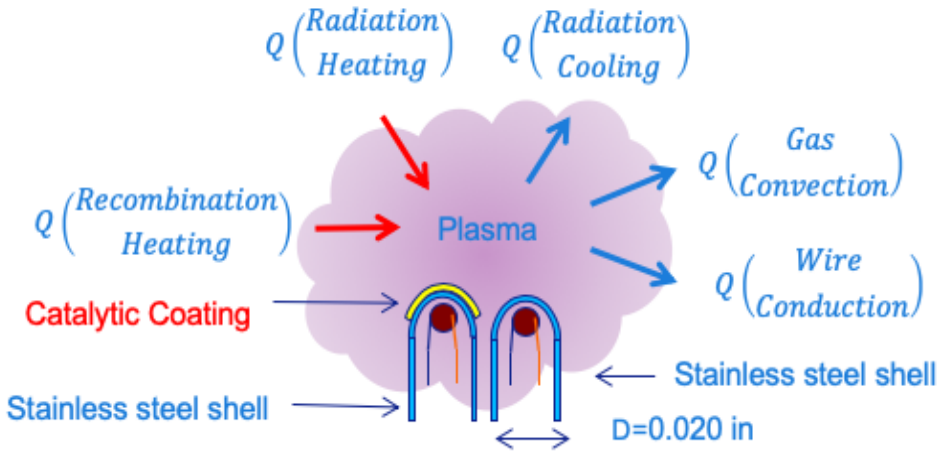

Figure 2.2: Radical probe principle schematics and heating and cooling mechanisms around the probe.

The left hand side of equation 2.1 is responsible for probe heating and the right hand side is responsible for probe cooling. Radical probes are encased in ceramic tubes besides the probe tip where the catalytic material is coated. Therefore, equation 2.1 takes into account only tip of the probe, where the probe is the hottest and this assumption, which is fulfilled during experiments, limits probe operation due to the fact that probe body remains relatively cooled during experiments. In such case, one can substitute values for thermal emission and conductivity in equations 2.2 and 2.3.

$$P_{thermal\,conduction} = \frac{13[\frac{W}{mK}] * S[m^2] * 100[K]}{0.3[m]} \tag{2.4}$$

$$P_{thermal\,emission} = 0.5 * 5.6 * 10^{-8} \frac{W}{m^2 K^4} * 100^4 [K^4] * S \tag{2.5}$$

Here, for temperature range below 300K, thermal conductivity is greater than thermal emissivity. Each radical probe system consists of two probes as mentioned above, therefore:

$$\frac{n W_D v A \gamma_{probe\,A}}{8} = \frac{\chi S}{l}(T_{cold\,probe\,A} - T_{hot\,probe\,A}) \tag{2.6}$$

$$\frac{n W_D v A \gamma_{probe\,B}}{8} = \frac{\chi S}{l}(T_{cold\,probe\,B} - T_{hot\,probe\,B}) \tag{2.7}$$

Since the probes are encased in double bore ceramic tubes their probe body temperature is the same, $T_{cold\,probe\,A} = T_{cold\,probe\,B} = T_{cold}$. By subtracting equation 2.6 to 2.7:

$$n\frac{W_D v A}{8}(\gamma_{Probe\,A} - \gamma_{Probe\,B}) = \frac{\chi S}{l}((T_{cold} - T_{hot\,probe\,A}) - (T_{cold} - T_{hot\,probe\,B})) \tag{2.8}$$

$$n = \frac{8 S \chi}{W_D v A} \frac{(T_{hot\,probe\,B} - T_{hot\,probe\,A})}{(\gamma_{Probe\,A} - \gamma_{Probe\,B})} \tag{2.9}$$

In equation 2.9, it is shown that radical density is proportional to the difference of temperature of two probes, stainless-steel probe which serve as reference probe and catalytic probe. Catalytic materials vary in reactivity with different radicals. In this particular study, radical density of hydrogen, oxygen and nitrogen were measured. Copper as catalytic coating was used for nitrogen and oxygen, gold for hydrogen since they have high recombination coefficient for their respective gases compared to stainless-steel. This idea can be expanded for multiple probe array with various catalytic materials as long as they are in close proximity ($< 1\,cm$) with each other. Here, the condition is that presence of at least one stainless-steel probe must be present. Such array has the capacity of measuring radical densities of different gas mixtures present in the vacuum system.

Recombination coefficient represents one of main drawbacks of this measurement method. Recombination coefficient is defined as the ratio of atoms striking the surface and reacting to the total number striking the surface [21], also known as $Haftungskoefficient$ defined by F.A Paneth and K.F Herzfeld [22]. Currently, two mechanisms of recombination are adopted,namely, Eley-Rideal (ER) and Langmuir-Hinshelwood (LT). ER states that direct reaction of ad sorbing an atom on the surface with an atom from gas phase and LT states that recombination involves only surface adatoms [23] [24]. The underlying reason is due to the fact that recombination of radicals on the surface depends on numerous factors such as temperature, pressure, impurities present, chamber size, surface morphology and coating thickness. Such factors play key roles in energy transfer mechanisms of association, dissociation and collisional energy transfer in low pressure regimes [24]. Impurities poison catalytic surface and probe response to the temperature charges decreases over time. Additionally, oxide and nitride layers are formed when probes are exposed to nitrogen and oxygen plasma. Over time thickness of catalytic material decreases (usually $1m$ thick) mostly due to sputtering processes. Due to such effects, a systematic and consistent process of re-coating the probes via magnetron sputtering is necessary, see subsection 3.2, in order to maintain consistency in experimental results, also, this translates to probe lifetime to amount to total of about two hours of plasma exposure before degradation starts. Nevertheless, the greatest uncertainty comes from gradient of neutral gas temperature during experiment. High neutral gas temperature in the plasma will yield lower total number density in the discharge thus overestimating generation of radicals which gives a higher recombination coefficient, [20] [25].

Next, a step-by-step radical density measurement procedure is outlined. A case study is chosen is of oxygen plasma at 30mT of pressure and 900W of RF power. One probe is bare stainless-steel and the other one is coated with copper catalytic material. Initially, temperature of both probes are the same as shown in **figure 2.3**, then oxygen plasma is turned on at 75 seconds which gives rise to the both probes' temperatures such that temperature difference is noticed, immediately. After some time, temperatures reach steady state

conditions. Radical density is calculated from average temperature difference between the probes via equation 2.9.

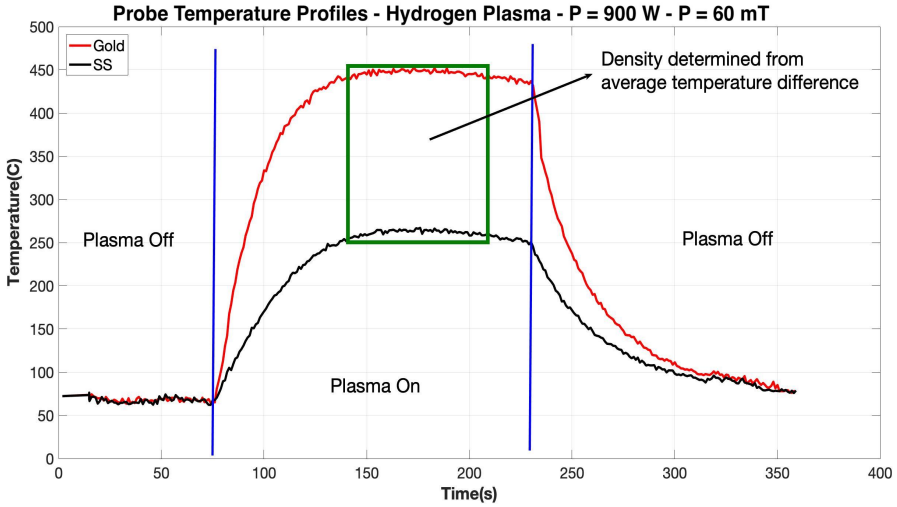

Figure 2.3: Temperature profiles for gold and stainless-steel coated catalytic probes for 900W and 60mT. Temperature difference is calculated from steady state region shown in green box.

s

For this study case, recombination energy of hydrogen radicals is $W_H = 4.52eV$, thermal conductivity of the probe body (stainless-steel) $\chi = 15\,W/m/K$, cross-sectional area of the probe is $2.12 * 10^{-7}m^2$ which is equal to the surface area of the catalytic material, average thermal velocity is $2296\,m/s$. Recombination coefficient of hydrogen radicals on gold surface is on average 0.24 [26] whereas on stainless-steel surface is 0.07 [18]. Substituting these values in equation 2.9:

$$n = \frac{8 \times 15W/m/K}{15eV \times 2296m/s} \frac{(447C - 262C)}{(0.24 - 0.07)} = 8.45 \times 10^{13}/cm^3 \tag{2.10}$$

In order to find the error of the measurement, general error propagation formula is used such that $\delta T_{Au=SS} = 1.5C$, $\delta v = 56m/s$, $\delta\gamma_{Au} = 0.1$, and $\delta\gamma_{SS} = 0.01$.

$$\delta n = \sqrt{(\frac{\delta n}{\delta T}\delta T)^2 + (\frac{\delta n}{\delta v}\delta v)^2 + (\frac{\delta n}{\delta T_{Au}}\delta T_{Au})^2 + (\frac{\delta n}{\delta T_{SS}}\delta T_{SS})^2 + (\frac{\delta n}{\delta \gamma_{Au}}\delta \gamma_{Au})^2 + (\frac{\delta n}{\delta \gamma_{Au}}\delta \gamma_{Au})^2} \tag{2.11}$$

$$\delta n = 1.183 \times 10^{13}/cm^3 \tag{2.12}$$

Thus, hydrogen radical density for 60mT at 900W is $8.45 \pm 1.182 \times 10^{13}/cm^3$

2.2 Magnetron Sputtering

Magnetron sputtering was the technique used to coat probes with catalytic films. Deposition of radical probes were carried out in a separate chamber and then transferred in Hydrogen Atom Radical Probe (HARP) chamber. Magnetron sputtering is a physical vapor deposition (PVD) process during which a magnetic and electric field is generated on the top of sputtering target. Low pressured gas inside the vacuum chamber is ionized by electric field to generate plasma. When the ionization occurs, neutral atoms are separated from electrons which then are trapped in the magnetic field. Trapped electrons near the target accumulate a high density and are responsible for higher ionization efficiency. Ionized gas is accelerated towards the target and the phenomenon of ion bombardment occurs. During ion bombardment, ions hit the target and transfer their energy to the surface atoms of the target, once this energy reaches higher then binding energy of target surface atoms then these atoms will be removed or sputtered [7]. A simplified picture of the magnetron magnetic field lines is shown in **figure 2.4a**. These magnetic field lines confine the electrons through what is known as a magnetic mirror configuration. Although not derived here, a magnetic mirror is a phenomenon that results in charged particles being reflected from high density magnetic fields to low density magnetic fields. Or in other words, a charged particle will be reflected from stronger magnetic fields to lower magnetic fields. When this magnetic mirror concept is

applied to the magnetic field lines shown in **figure 2.4a** it results in electrons reflecting from regions where the field lines are closely spaced. Therefore, as the electrons gyrate around and move along the magnetic field lines, they will encounter strong magnetic fields in the middle of the target and on the outer edges. Consequently, electrons will then be reflected back to the lower density magnetic field between those two positions. This will effectively confine the particles in a band around the target, this is known as a racetrack. It is given this name because the E X B drift will cause the electrons to drift around this band. This well-confined racetrack has significant consequences on the sputtering of the target. Since the electrons are well-confined within the racetrack the majority of ionizations will occur within this region. As gas molecules are ionized, they will be accelerated toward the target due to formation of the plasma sheath. These accelerated ions will then impact the surface and sputter off material. Since the ions are accelerated perpendicularly to the target from the position of their creation, the racetrack profile will result in enhanced material erosion from this region of the target. This erosion pattern is shown on **figure 2.4b**, where the lighter shaded region represents larger material erosion.

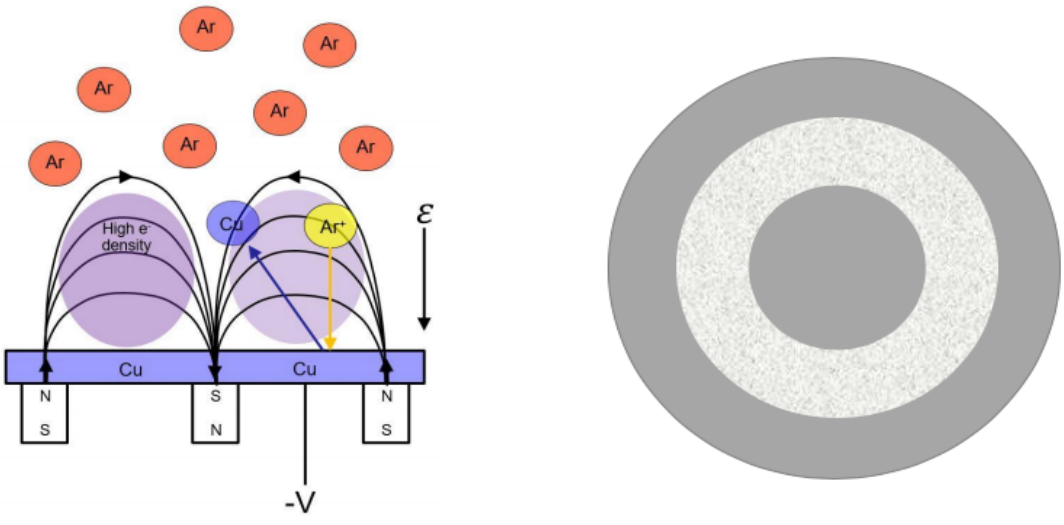

(a) Conventional Magnetron (b) Sputtering Erosion Pattern "Race Track"

Figure 2.4: Simplified representation of magnetic field lines from conventional magnetron [7].

2.3 Helicon Plasma

Helicon waves are propagating whistler wave modes, which are generally excited by RF antenna, in a finite diameter, axially magnetized plasma column [27]. These waves are coupled with transverse mode structures inside the vacuum chamber. Transverse mode propagates down the cylindrical plasma chamber and the mode is absorbed by electrons due to collisionless and collisional damping. Helicon waves have frequencies between the lower hybrid frequency $(\omega_C \Omega_C)^{1/2}$ and the ion plasma frequency Ω_p, and thus much lower than the electron cyclotron frequency ω_c [8]. Electromagnetic fields have modes in axial, radial and azimuthal variation and they generally propagate in low magnetic field, low-frequency and high-density regime which is characterized [27]:

$$\omega_{LH} \ll \omega \ll \omega_{ce} \tag{2.13}$$

$$\omega_{pe}^2 \ll \omega \omega_{ce} \tag{2.14}$$

Where ω_{LH} is the lower hybrid frequency, ω_{pe} is electron plasma frequency and ω_{ce} is electron gyro-frequency. Frequency used in industry and research is 13.56MHz in terms of discharge processes with magnetic field varying from 100G to 1000G which generate plasma densities with a range between $10^{11} cm^{-3}$ up to $10^{14} cm^{-3}$. Maxwell's equations help to understand theoretical operating principle of helicon waves [10]:

$$\nabla \times E = \frac{\partial B}{\partial t} \tag{2.15}$$

$$\nabla \times B = \mu_0 j \tag{2.16}$$

$$E = \frac{1}{e n_0} j \times B_0 \tag{2.17}$$

Where E and B are the electric and magnetic field, respectively; μ_0 is free-space perme-

ability, n_0 is density at equilibrium, B_0 is magnetic density at equilibrium, j is the current density and e is elementary charge. Displacement current is neglected in equation 2.8 and plasma current is carried out by $E \times B$ guiding center drift of the electrons [10]. Based on equations 2.6 and 2.7 motion of the ions can be neglected because electron's cyclotron motion and whistler wave angular frequency is very high. Assuming the waves are of the form $e^{i(m\theta+kz-\omega t)}$ and such waves propagate in $B = B_0\hat{z}$. Then dispersion relations for whistler wave and electromagnetic electron cyclotron wave are, respectively:

$$\omega = \frac{k_0^2\omega_{pe}^2}{\beta k_z \omega_{ce}} \tag{2.18}$$

$$\beta = \frac{\omega}{k}\frac{n_0 e\mu_0}{B_0} \tag{2.19}$$

Where β is defined as wave-vector magnitude such as $\beta^2 = k_\perp^2 + k_z^2$. This is based dispersion relation for helicon waves which shows that phase velocity varies with density and magnetic field [9]. HARP chamber is a cylinder shape, therefore, boundary condition for waves with $ka \ll 1$ is [9]:

$$m\beta J_m(k_\perp a) = 0 \tag{2.20}$$

Where a is radius of the cylinder, and lowest radial mode with m=1 antenna which is the case with most experiments give $k_\perp a$ as a Bassel root solution of 3.83 as shown in equation 2.21 such that for any given mode, density is proportional to B [8].

$$\frac{3.83}{a} \propto \frac{\omega}{k}\frac{n_0}{B_0} \tag{2.21}$$

On other hand, electron cyclotron wave propagates at given angle to magnetic field such that it is called TG mode [9]. Combining Maxwell's equations above with electron equation of motion 2.22 gives 2.23:

$$F = q(E + v \times B) \tag{2.22}$$

$$\delta \nabla \times \nabla \times B - k \nabla \times B + k_w^2 B = 0 \tag{2.23}$$

Where $\delta = (\omega + i\nu)/\omega_c$, $k_w^2 = \omega n_0 \mu_0 e / B_0$ and ν is collision frequency of electrons with ions and neutral [8]. Equation 2.23 can be factored and solutions for $\delta k_w^2 \ll k^2$ are 2.24:

$$\beta_{1,2} = \frac{k}{2\delta}\left[1 \mp \left(1 - \frac{4\delta k_w^2}{k^2}\right)^{1/2}\right] \approx \frac{k}{2\delta}\left[1 \mp \left(1 - \frac{2\delta k_w^2}{k^2}\right)\right] \approx \begin{pmatrix} k_w^2/k \\ k/\delta \end{pmatrix} \tag{2.24}$$

Lower positive sign represents TG mode and upper negative sign represent H-more. Generally, RF energy is mostly absorbed by TG-mode rather then H-more because TG-more has large β but short wave length and it is localized near boundaries. It is shown [8] that TG-mode affects the current density more then magnetic density and its amplitudes are peaked near the edge. Helicon waves give very unique mode patterns for varying azimuthal wave numbers. Below are examples for modes $m = \pm 1$ and $m = 0$. Mode $m = -1$ has a narrow profile which is cause for mode's weaker propagation and for mode $m = 0$ the pattern changes from electromagnetic to electrostatic for every each half-cycle [8], see **figure 2.5**.

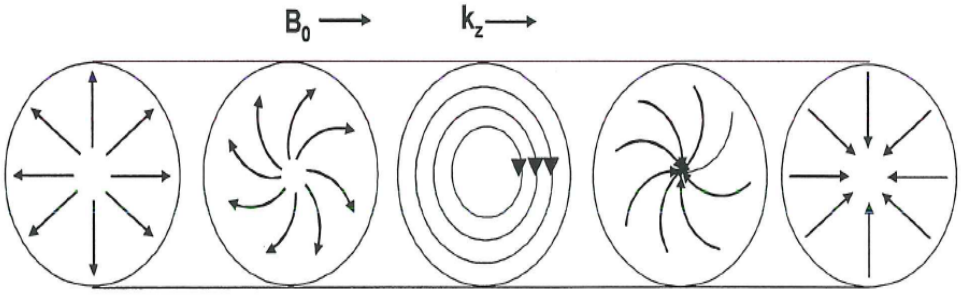

Figure 2.5: Traverse electric field lines of helicon plasma source for mode m=0

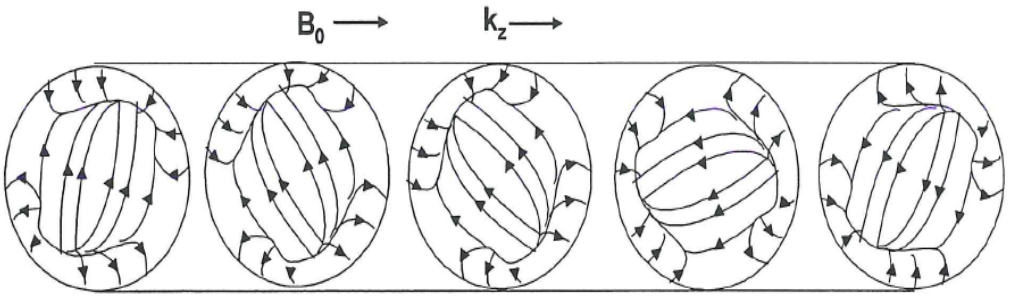

Figure 2.6: Traverse electric field lines for mode m=1,, which rotates clockwise as observed by stationary point [8]

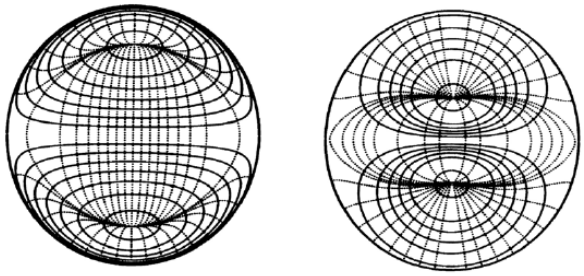

Figure 2.7: Electric field patterns for m = +1 (left) and m=-1 (right) modes [9]

2.4 Langmuir Probe

Langmuir probe is one of most commonly used diagnostics to determine basic plasma parameters, it consists of a wire immersed in plasma and it measures current for various voltages applied. The probe is a intrusive method of determining electron temperature, electron density, electron energy distribution function and ion density. Voltage and current collected by a Langmuir probe generate an I-V trace as shown **figure 2.8** which normally reversed but for analysis and conventional purposes the y-axis is switched since ion current is considered to be positive and electron current is negative, the I-V trace is used to analyze and determine plasma parameters. Probe is biased with voltage V with respect to ground in order to draw current. Langmuir probe measures total current which consists of ion current and electron current.

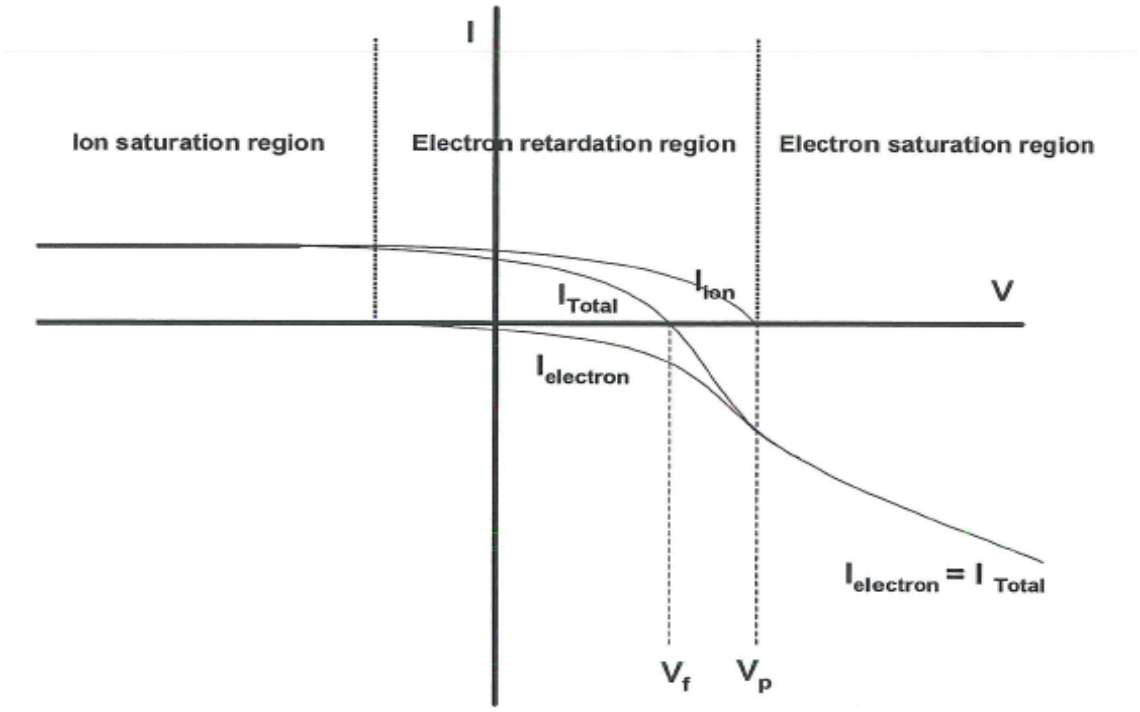

Figure 2.8: Langmuir probe trace for cylindrical probe geometry shown with three characteristic regions: ion saturation region, electron retardation region and electron saturation region [10].

The I-V trace consists of three regions: ion saturation region, electron retardation region and electron saturation region. On the right side of I-V trace, the region where potential is the lowest is called ion saturation current because total current equals ion current and no electrons travel to the probe. Ion saturation current is useful for determining plasma density. As voltage is increased, probe current it becomes more negative as only highly energetic electrons reach the probe while low energy electron [11]. When bias reaches floating potential, $V = V_f$, total current is equal to zero. In the region between plasma potential and floating potential, electrons are repelled according to Boltzmann relation and thus it is called electron retardation region and since the number of electrons collected depend on energy, electron energy distribution function is obtained from this region. Also, if the electron energy distribution function is a Maxwellian or Druyvesteyn then electron temperature can be calculated as well. At plasma potential, electrons can travel freely at the probe without any

potential drop to retard them [11]. As voltage increases beyond plasma potential, currents will saturate due to domination of electrons. Since no ions reach the probe at this region, theoretically electron density can be derived from this region however it is not credible measurement. Electron saturation depends also on the shape of probe tip, in our case cylindrical probe tip is used.

Plasma environment can come in many variations, therefore, based on plasma regime appropriate information regarding plasma parameters can be obtained. Plasma regime can easily be determined based on probe radius, Debye length and mean-free path [10]. The detailed Langmuir probe trace analysis below is based on Dr. D.N.Ruzic's book. Floating potential is found at the location where the current is zero then in order to evaluate plasma potential one should take the derivative of the current with respect to voltage and find the minimum value above floating potential. Often, RF noise generated elsewhere in the lab distorts data, therefore, either a filter is needed or a polynomial fit. To determine two most important parameters such as electron temperature and electron density it is detrimental to take into account plasma regime and sheath size since the following calculations depend on them. Sheath is the space around the probe which establishes a voltage barrier due to the flux of ions and electrons to the surface [11]. Sheath size varies and it depends on Debye length which is the scale over which electrons screen out electric field and it a a characteristic distance over which significant charge separation can occur. Empirical Debye length is show in equation 2.25.

$$\lambda_D = 7430\sqrt{\frac{T_e}{n_e}} \tag{2.25}$$

where n_e is electron density in m^{-3} and T_e is electron temperature in eV. Based on [11], sheath size is estimated by multiplying equation 2.25 by four. If the sheath size is greater then probe radius then sheath is considered to be thick and if the sheath size is less then probe radius then sheath is thin. Thin regimes assumes that sheath size is approximately the size of probe radius such that any particle entering the sheath is collected by the probe.

On the opposite, in the thick regime, incoming particles could be deflected around the probe area due to potential gradient and if the particle is in close proximity to the probe, it could be attracted towards it, thus making effective area of the probe broader. Next step in Langmuir probe analysis is to determine collisionality of the plasma regime. Such regime can be either collisional plasma regime which means that collisions occur between neutral atoms and electrons within sheath space and collisionless plasma means little or no collisions. Mathematically, the collisionality of the plasma is determined by mean-free-path (mfp) which is defined as average distance before electrons or any particle travel before it collides and it is given by equation 2.26.

$$\lambda_0 = \frac{1}{n_0 \sigma} = \frac{kT}{p\sigma} = \frac{0.061}{P(mT)} m \tag{2.26}$$

where λ_0 is mean-free-path, σ is collision cross-section, n_0 is density of neutral atoms, k is Boltzmann constant, and P is pressure. After determining collisionality, one should process with finding electron current by subtracting ion current from total current of measured raw data.

$$I_i = \frac{ne}{4} \sqrt{\frac{8e}{\pi m_i}} A_p (1.127) \sqrt{V_{plasma} - V} \tag{2.27}$$

Equation 2.27 shows calculation of current I_i, where A_p is probe area, V_{plasma} is plasma potential, V is probe voltage, m_i is ion mass, n is density and e is electron charge. Once, electron current is known then electron temperature is found by taking natural logarithm which produces a straight line with a certain slope. Thus, the inverse proportional of the slope is electron temperature. Equation 2.28 describes the slope of the line. Note, one can estimate density by solving equation 2.27 for ion saturation current.

$$ln(|I_e(V)|) = -\frac{e}{kT_e}(V_{plasma} - V) + ln(|I_{esat}|) \tag{2.28}$$

where I_e is electron current and I_{esat} is electron saturation current. Additionally, electron

density is determined by Laframboise's numerical method which disregards sheath regime due to iterative nature of the method and it does solve Poisson's equation as shown in **figure 2.9**. Laframboise theory assumes an isotropic distribution of ions of a singe energy E_i [28] [29] and also extends calculations to a Maxwellian ion distribution at temperature T_i. Note, there are other methods to determine electron density such as Allen-Boyd-Raynold theory and Orbital Motion Limit theory [29].

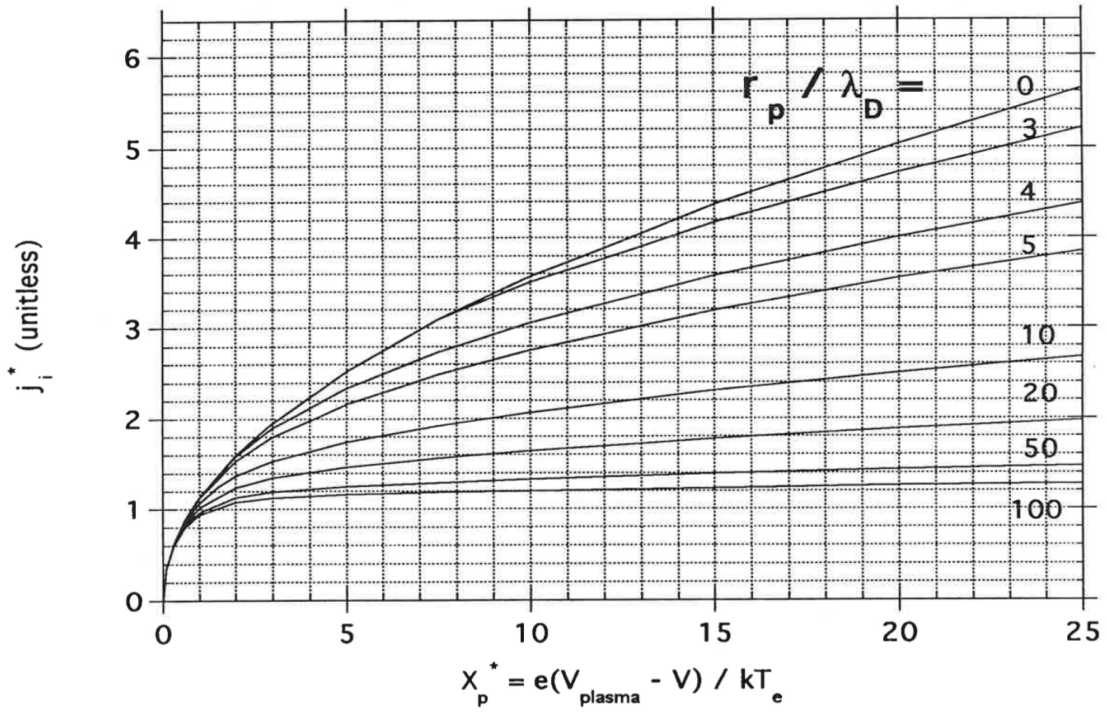

Figure 2.9: Laframboise graphical solution in dimensionless units for cold plasma [11].

Figure 2.9 shows that for large probes ($R_p/\lambda_D \gg 1$) ion current saturates due to thin sheath regime. For small R_p/λ_D, ion current increases as plasma voltage increases as the sheath radius increases [29]. In y-axis, Bohm acceleration in the pre-sheath (j^*) is taken into account and numbers in each curve are the ratios of probe radius and Debye length [11]. The x-axis is the ratio of voltage below plasma potential to electron temperature shown in equation 2.29 as $X*_p$.

$$X_p^* = \frac{e(V_p - V)}{kT_e} \tag{2.29}$$

Equation 2.25 required density to be known such that Debye length is calculated, however, equation 2.27 can be used to estimate this quantity. Since R_p/λ_D and $X*_p$ are known, j^* can be found graphically via Matlab script. Thus, ion current could be rewritten as:

$$I_i = \frac{en}{4}\sqrt{\frac{8kT_e}{\pi m_i}} A_{probe} j^* \tag{2.30}$$

Electron density can be found by equation 2.31:

$$n_e = 1.05 \times 10^{15} \sqrt{\frac{\mu}{T_e}} \frac{I}{A_{probe}} \tag{2.31}$$

where μ is gas mass in amu. Note, initial density was assumed, therefore, the process must be iterated such that a convergence is achieved.

Next, a detailed example of Langmuir probe analysis is shown. Experiment with the same conditions as radical probe analysis is chosen as the study case. **Figure 2.10** shows raw data of the I-V trace for 900W at 60mT.

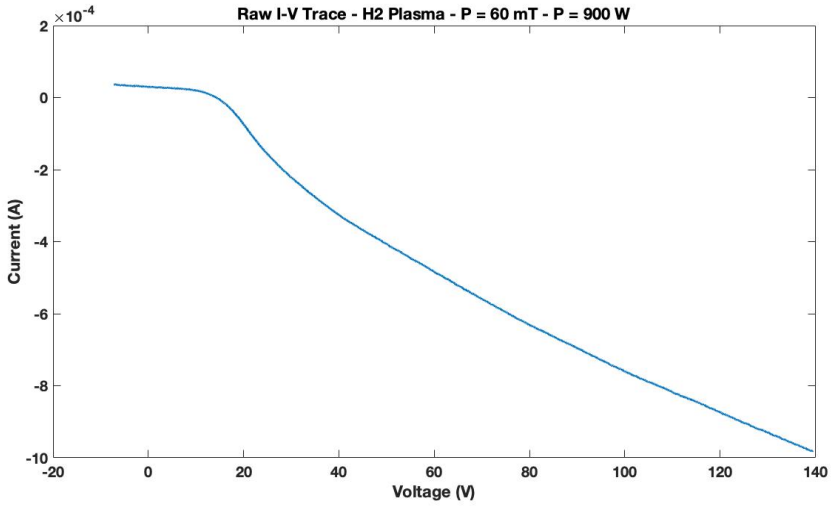

Figure 2.10: Raw I-V trace Langmuir probe generated for study case with experimental parameters of 900W at 60mT.

First step in the analysis process is to determine length scale regime in which data is obtained. Based on equation 2.25, Debye length is $3.69 \times 10^{-6}m$ by assuming appoximation of electron temperature of $3eV$ to and electron density of $5 \times 10^{15}/m^3$, then sheath length is defined as $4 \times \lambda_D = 1.4671 \times 10^{-5}m$. Probe radius is $r_P = 0.127 \times 10^{-3}m$. Mean-free-path is calculated from equation 2.26, where the pressure is 60mT, such that $\lambda_0 = 1 \times 10^{-3}m$. Length scale is then determined by comparing above three calculated lengths, such that $4\lambda_D < r_P < \lambda_0$ which shows that this study case took place in collisionless thin sheath regime.

In the next step, plasma potential is determined by finding minimum of first derivative dI/dV of IV trace, for this case plasma potential is $V_P = 20V$. Since the total current is sum of electron and ion currents, a fit of ion saturation region is needed in order to subtract ion current contribution, see **figure 2.11**.

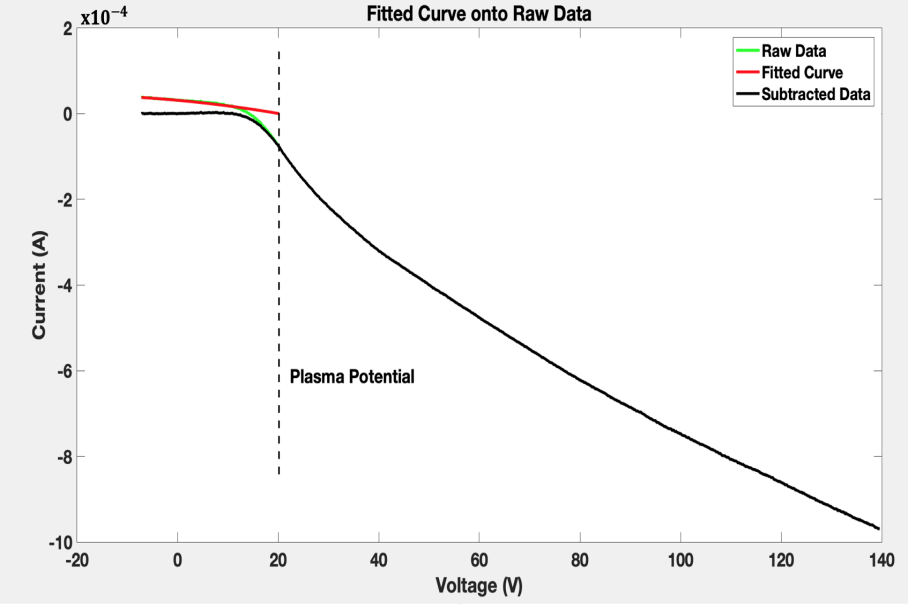

Figure 2.11: A curve which is forced to zero at plasma potential is fitted to raw data in order to remove ion current contribution for a collisionless thin sheath regime study case.

Another characteristic point in IV trace is floating potential which is found when current equals zero ($y = 0$), meaning ion and electron currents are equal thus floating potential is $Vp = 14.1V$. Electron temperature is determined from taking natural logarithm of current

and plotting it vs voltage. A straight line is drawn between plasma voltage and floating potential who's inverse slope yields electron temperature, $Te = 1/m$, see **figure 2.12**. Thus, electron temperature is 3 eV. If the slope is perfectly linear, then Maxwellian electron energy distribution is indicated, realistically, the slope will rarely be perfectly linear.

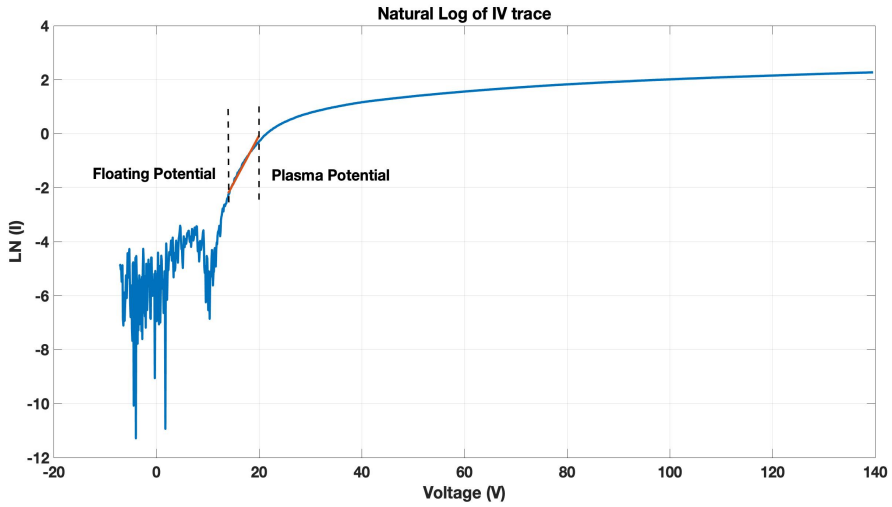

Figure 2.12: Natural log of I-V trace plot and red line plotted in between plasma potential and floating potential whose inverse slope equals electron temperature.

Next, electron density will be determined for collisionless thin sheath regime via equation:

$$n_e = 1.05 \times 10^{15} \sqrt{\frac{\mu}{T_e}} \frac{I}{A_{probe}} = 1.05 \times 10^{15} \sqrt{\frac{2\ amu}{3eV}} \frac{0.8 \times 10^{-6} A}{2.25 \times 10^{-5} m^2} = 3.05 \times 10^{13} / m^3 \quad (2.32)$$

Chapter 3

Experimental Setup

The development and the study of radical probe system was funded by Apple Inc. and it was conducted at Center for Plasma and Material Interaction laboratory at University of Illinois. This chapter consists overview description of vacuum system, magnetron sputtering chamber, radical probe system, and Langmuir probe system. Additionally, a software is developed for in-situ measurements of radical densities.

3.1 HARP Vacuum System

The study of radical probe system was conducted in Hydrogen Atom Radical Probe (HARP) vacuum system which was previously Plasma-Quest 256 reactor. HARP chamber consists of few systems including main vacuum chamber which has a plasma diffusion volume of $1.29 \times 10^5\ cm^3$, PTM M∅RI 200 Helicon plasma source, radical probe holder, pumping system and gas delivery system. HARP system is shown in the **figure 3.1**. HARP is equipped with a rotary vane rough pump and a powerful 1600 l/s turbo-molecular pump which yields a base pressure in high 10^{-8} torr. Gas delivery system is computer controlled by four mass flow controllers.

Essential part of HARP system is PMT M∅RI 200 helicon plasma source. M∅RI 200 operates at 13.56 MHz frequency with a 180° phase difference and power output from 0-3 kW, antenna loops has 11 cm diameter and are separated by 12.7 cm distance. Mode of the antenna for this study is m = 0 such that magnetic field coils give shape of static magnetic field lines which are controlled by varying the current of each coil. In order to limit radial

diffusion of plasma in the chamber, a multi-pole magnetic bucket is installed [10]. M⌀RI 200 helicon source has an integrated automatic matching network which serves to maximize power delivery efficiency. Additionally, M⌀RI 200 has the capability to produce helicon plasma with presence of magnetic fields and inductively coupled plasma without presence of magnetic field.

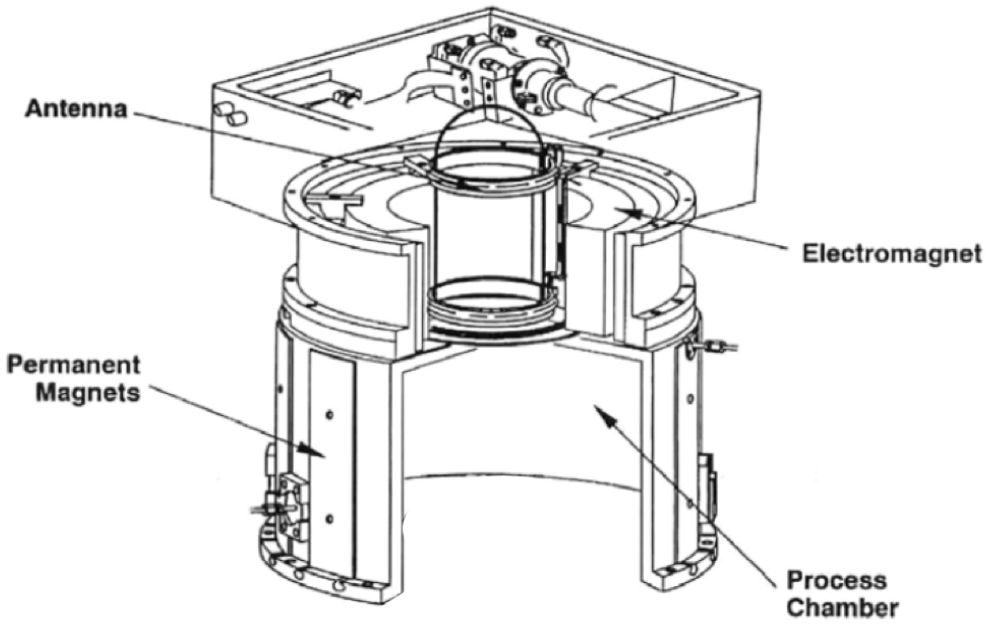

Figure 3.1: PTM M⌀RI 200 Helicon Source with matching network [8].

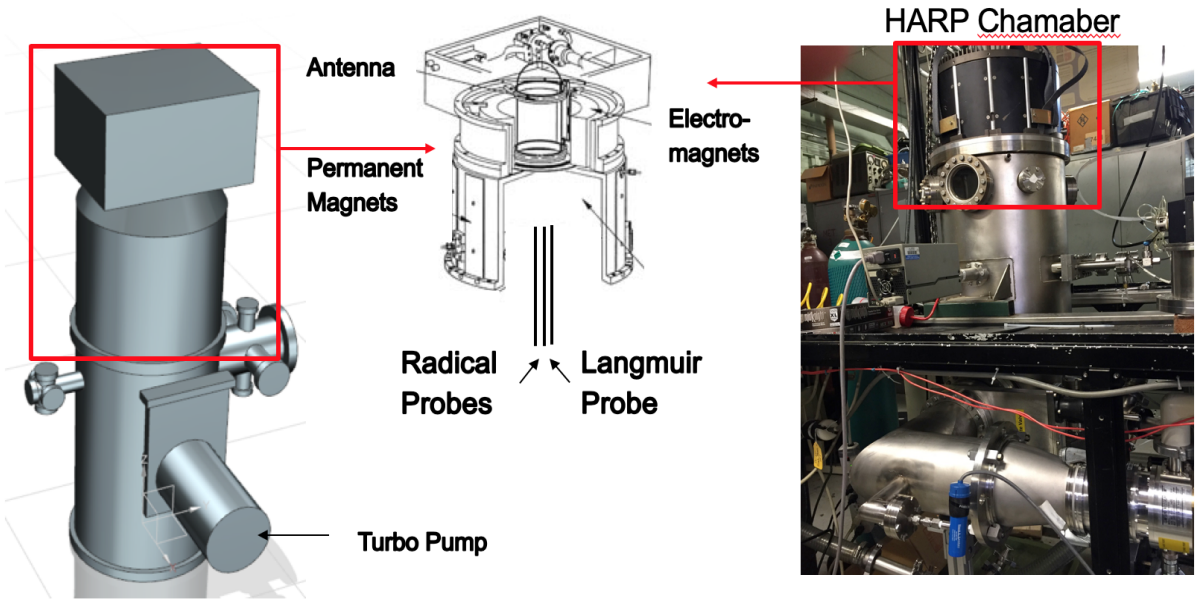

Figure 3.2: HARP Chamber

3.2 Magnetron Sputtering Chamber

Magnetron sputtering chamber consists of two magnetron guns and it has two sub-chambers, each sub-chamber has its own gas delivery system, pressure gauge and cooling system. Upper chamber has a three-inch mangetron gun and it is mainly used to deposit various thin films on different substrates/wafers which includes a load-lock system equipped with transferable arm in order to insert and transfer the samples in desired position. Lower chamber has a two-inch magnetron gun and it is solely used for depositing catalytic thin film on probe tips. K-type thermocouples are cased by ceramic tubing in order to ensure that catalytic material is deposited only on the probe tip, also thermocouples are inserted horizontally such that minimal damage is done to the probes. Magnetron sputtering gun is biased by a DC power supply that is capable of delivering 2000V at 100mA at maximum output power, however, for deposition purposes of catalytic materials 1000V at 50mA are

used. Ceramic cased thermocouples were placed in 1 inch distance from magnetron for time interval between 6 to 10 minutes, this recipe yields a few microns thick catalytic layer on probe tip.

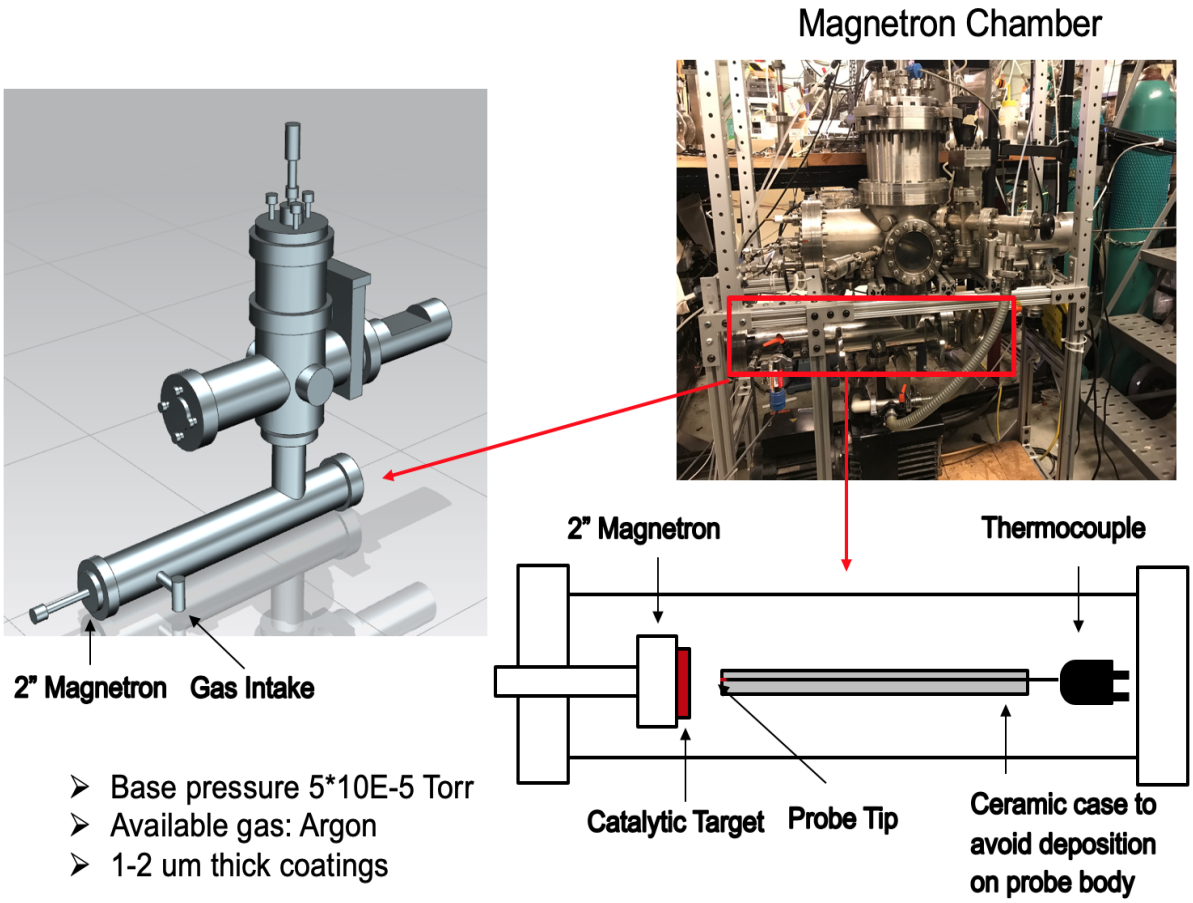

Figure 3.3: Magnetrgon Sputtering Chamber

3.3 Radical Probe System

Radical probe system consists of a probe array holder which holds up to six probes and can be mounted in any direction given proper space. However, for different mounting configurations the number of probes is theoretically unlimited. In HARP chamber, probe array is mounted in vertical position and it has the capability to move in r and z direction. Radial position is controlled via linear motion feed-through which is commanded by in-situ measurement software. Z direction is controlled manually and it has the capability to enter

the ceramic dome of helicon plasma source where the density is the highest if need be. Radical probes mounted in probe array are generally cased in ceramic rods thus cooling and heating mechanisms are identical for all probes. Additionally, radical probe tips are mounted in same spatial proximity to ensure consistent results. Probes are K-type with thermal response of only few milliseconds and they can come in various lengths. For each radical density measurement two probes are needed as explained in section 2.1, different gas mixtures can flow inside the chamber since each gas (nitrogen, oxygen and hydrogen) activates different recombination coefficient for each catalytic material. **Figures 3.4** and **3.5** show probe array assembly and **figure 3.6** shows schematic of thermocouple with catalytic coating. Densities are measured for hydrogen, oxygen and nitrogen as individual gases as well as mixed with varying pressure and power.

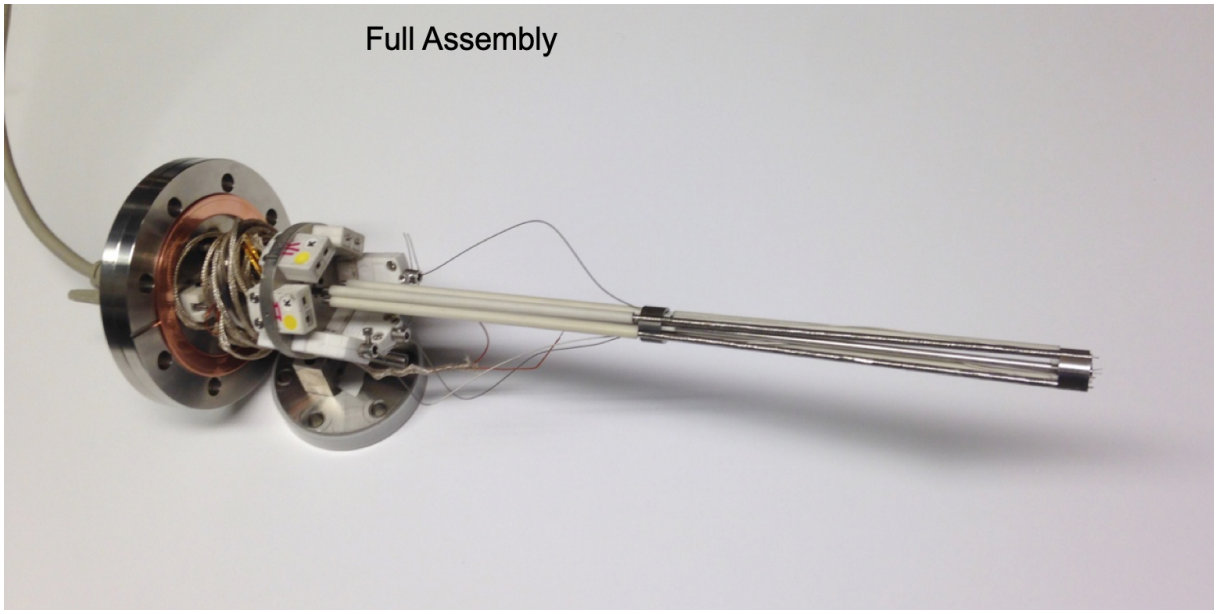

Figure 3.4: Full assembly with six radical probes connected to 4 1/2 ” flange.

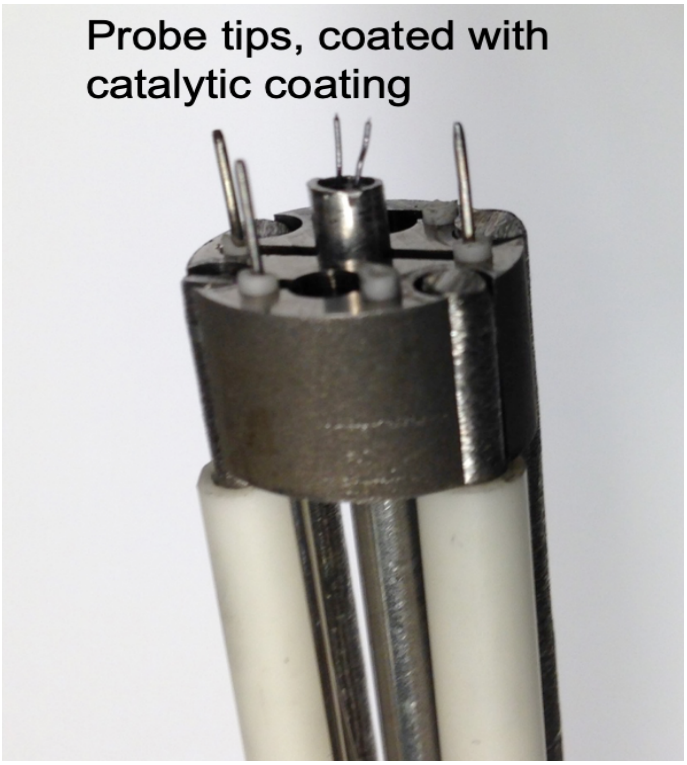

Figure 3.5: Six radical probe assembly system with Langmuir probe in the center.

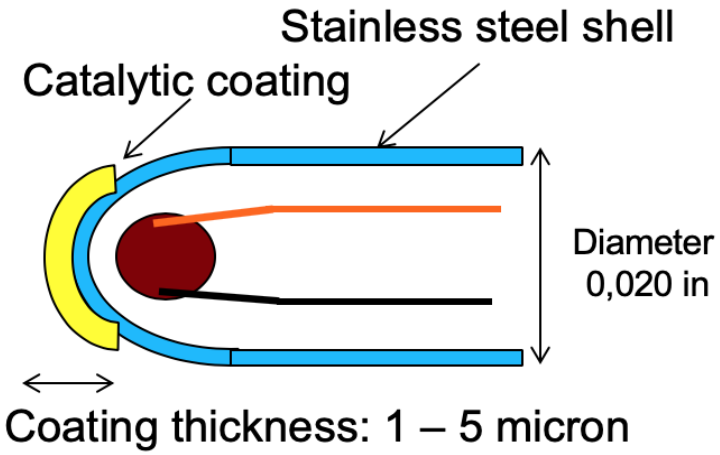

Figure 3.6: Schematic of thermocouple with catalytic coating.

Lifetime of radical probes specifically catalytic surface degradation highly depends on vacuum conditions, chamber contamination and the fact that radical species cause surface properties to change [16]. Lifetime of radical probe system in HARP is usually three hours. However, probe surface cleaning could be achieved by applying a bias which causes con-

tamination layer on the probe tip to sputter via ion bombardment. Argon gas is used to sputter clean probe tip. Additionally, if probe shows signs of high contamination then a long sputtering process is used to remove all the catalytic material from the probe tip and then magnetrgon sputtering is used to redeposit new catalytic coating.

Essential part of radical probe system is the Ra-Den software which measures in-situ radical densities based on the equations in section 2.1, namely equations 2.5 and 2.5. Ra-Den as integral part of radical probe system is developed in LabView using a data acquisition (DAQ) device. Radical probes are temperature-dependent voltage devices due to thermo-electric effect which results from two different electric conductors forming an electric junction. Voltage signal given in millivolt is converted to unipolar analog signal via DRSL-TC signal conversion op-amp. For each probe an electrical connection is established between DRSL-TC signal conversion device and DAQ device which in turns it is connected to computer via USB cable. Below, **figure 3.7** shows user interface of Ra-Den software.

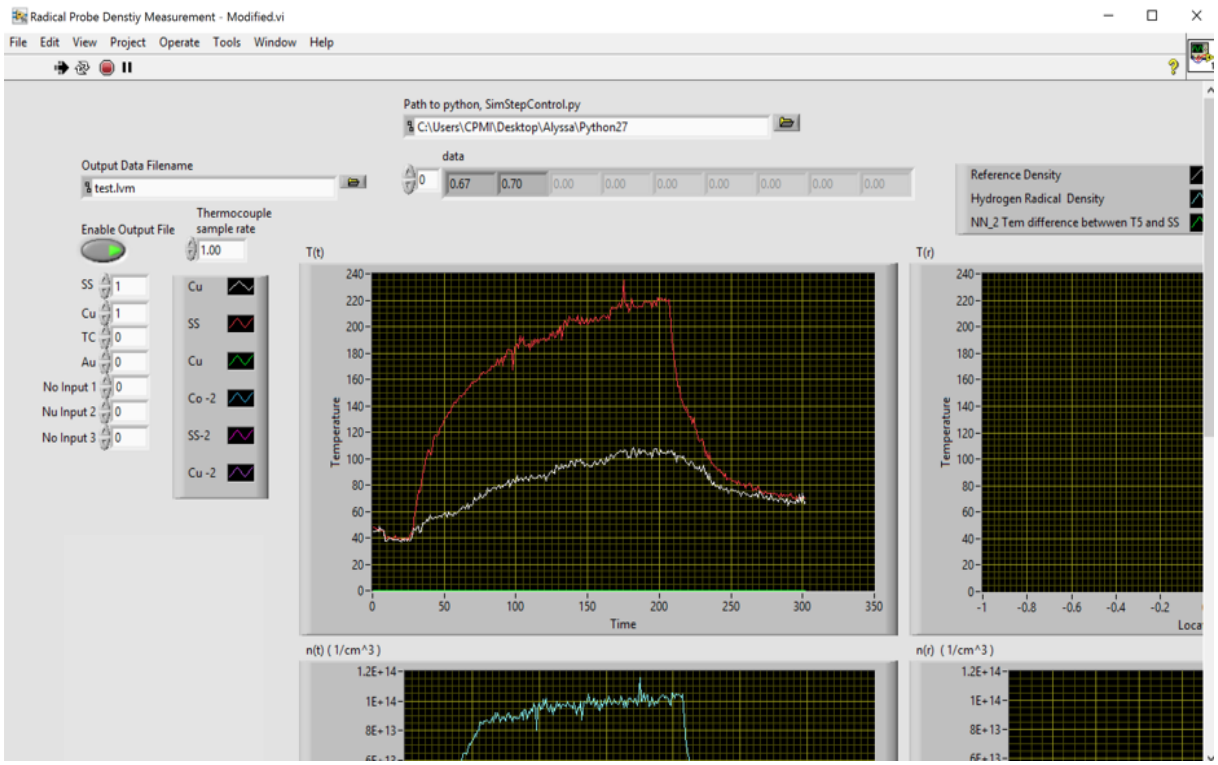

Figure 3.7: View of Ra-Den software while collecting data and showing temperature difference between stainless-steel and copper coated probes.

3.4 Langmuir Probe System

Langmuir probe is installed together with radical probes such that data is collected from the same spatial location. Langmuir probe consists of single tungsten wire cased by ceramic tube and it is connected via coaxial wire. Additional stainless-steel and ceramic tubes case the probe for grounding purposes. Langmuir probe schematic is shown in **figure 3.8**.

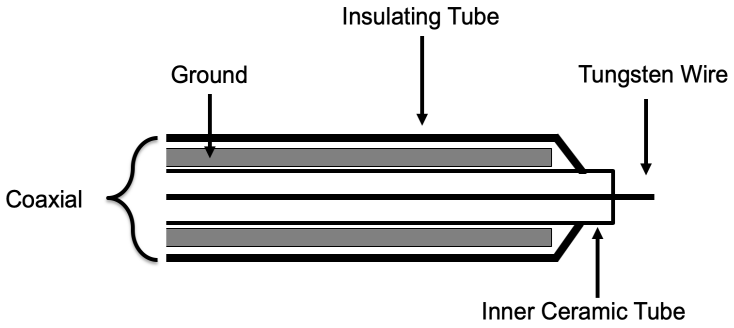

Figure 3.8: Schematics of in-house built Langmuir probe used during experiment.

External auxiliary devices of Langmuir probe consists of wave function generator, bipolar operational amplifier, resistor and oscilloscope. First, wave function generator outputs a wave with a voltage window of few volts, usually a triangular wave or seesaw, to bipolar op-amp power supply. The power supply amplifies the wave voltage to a window of $\pm 80V$ centered about a variable voltage. This enables to sweep entire voltage needed, from ion saturation region to electron saturation region, for I-V trace analysis Langmuir probe signal travels through BNC cable to a resistor (5.1 $k\Omega$ used), differential probes which are connected to oscilloscope are placed across the resistor to obtain current and voltage. Single Langmuir probe system is shown in **figure 3.9**.

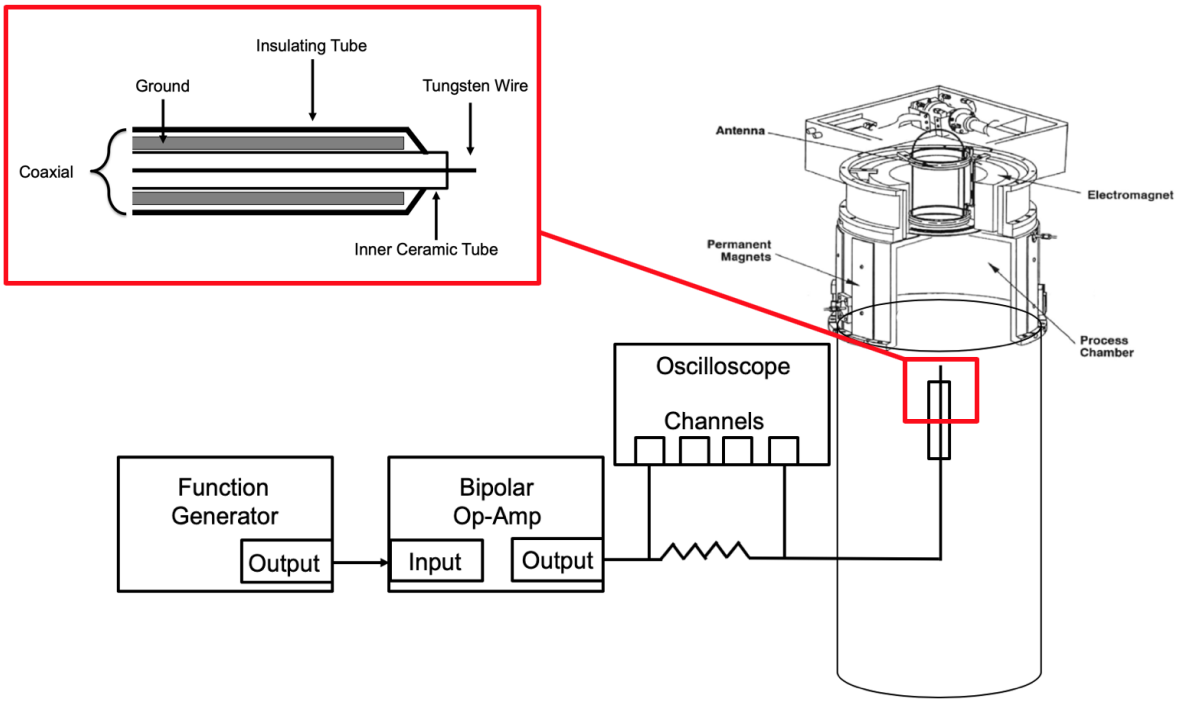

Figure 3.9: Schematics of integrated Langmuir probe system which includes a function generator, a bipolar op-amp and an oscilloscope in HARP chamber.

Chapter 4

Experimental Results

As above-mentioned, radical density of hydrogen, oxygen and nitrogen as individual gases and as mixed were measured via radical probes in HARP chamber. Additionally, electron density and electron temperature are measured via Langmuir probe as comparison to radical densities. Recombination coefficient of hydrogen radicals on gold surface is on average 0.24 [26] whereas on stainless-steel surface is 0.07 [18]. For oxygen radicals, recombination coefficient on copper surface is 0.17 [30] and for stainless-steel surface is 0.07 [31]. Lastly, recombination coefficient for nitrogen radicals on copper surface is 0.068 [32] [33] and on stainless-steel surface is 0.002 [33]. There is discrepancy in academia regarding recombination coefficients' values, however, tabulated values used (see table 4.1) to determine radical density are chosen closest to HARP chamber conditions. Recombination values are determined by two methods: catalytic probes or optical emission spectroscopy which rely on different theories and depend on temperature, flow rate, chamber geometry, surface morphology, lifetime and plasma source [34].

Table 4.1: Recombination coefficients' values used in calculating radical densities.

Selectivity	Recombination Coefficient
H on Au	0.24 [26]
H on SS	0.07 [18]
O on Cu	0.17 [30]
O on SS	0.07 [31]
N on Cu	0.068 [32] [33]
N on SS	0.002 [33]

Overall results show that electron density and radical density increase with power and pressure whereas electron temperature decrease with increasing pressure and increase with increasing power. Additionally, probe sensitivity is tested when exposed to mixture of gases in order to prove that combination pair of catalytic materials and gas can be differentiated accordingly. Furthermore, ionization and radical density percentage for each gas is compared to total ionization cross-section.

Additionally, a remaining issue regarding radical probe is contamination of catalytic material during operation as aforementioned in section 3.3. Contamination or poisoning of radical probes is result of nitride and oxide layers forming when probes are exposed to nitrogen and oxygen plasmas as well as impurities present in the chamber. Consequence of poisoning is response degradation of catalytic properties and decrease in probe ability to differentiate between gases when multi-probes are present and resulting in decrease of sensitivity to detect radicals. **Figure 4.2** shows a study case how copper coated radical probe losses its sensitivity to detect nitrogen radicals over time under the same experimental conditions due to above-mentioned reasons.

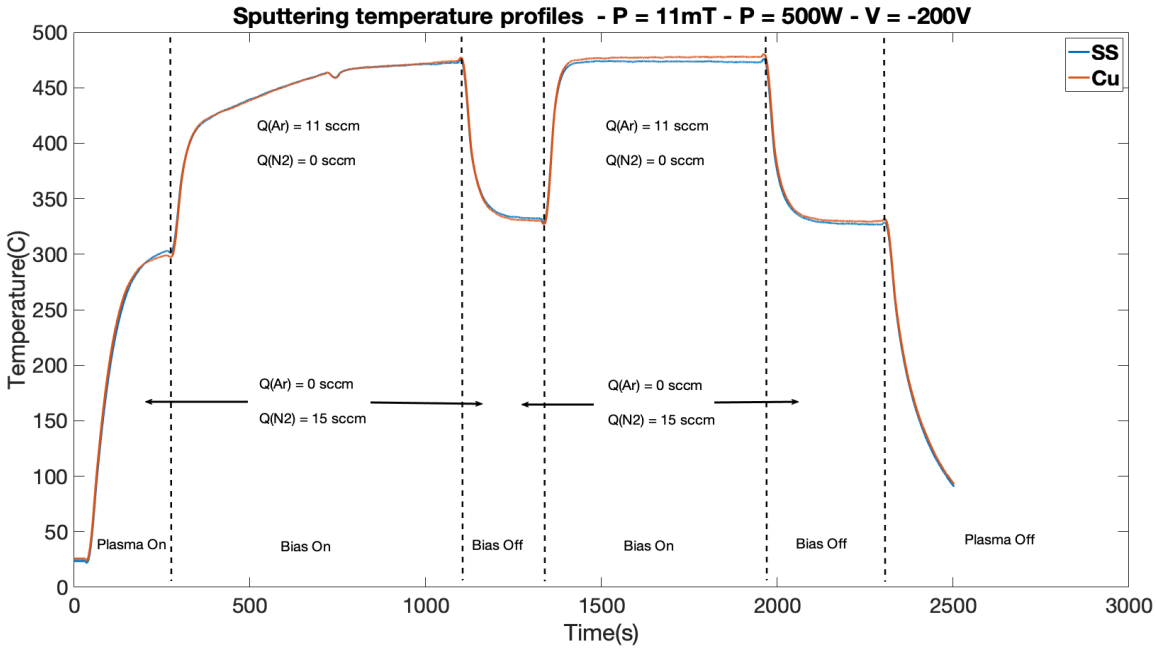

Figure 4.1: Sputtering temperature profiles of copper and stainless-steel probes. Argon plasma is used to sputter poisoned probes biased at -200V followed by nitrogen plasma in two cycles in order to test reactivity of the catalytic materials.

Etching is attempted by biasing the probes negatively such that positive argon ions are drawn to bombard the probe thus etch contamination layer off catalytic probes. **Figure 4.1** shows temperature profiles of copper and stainless-steel catalytic probes undergoing two cycles between argon plasma sputtering and nitrogen plasma to detect temperature difference. Both probes were previously exposed to nitrogen plasma for over three hours thus probes developed contamination layers which buried catalytic material under, therefore, no temperature difference is detected afterwards. In the first region of **figure 4.1**, nitrogen plasma is turned on and no temperature difference is observed, whereas normally for pristine probes temperature difference would be obvious, see **figure 2.3**. Next, a bias of -200V is applied to probes, nitrogen gas is cut-off and argon is flown in the chamber while maintaining total pressure constant. Temperature of probes rises significantly due to sputtering then bias and argon flow are turned off and nitrogen is introduced again. In the presence of nitrogen plasma after argon sputtering, probes do not show any temperature change thus this process

is repeated twice but no changes were observed. In-situ cleaning is difficult if at all to be achieved, thus once poisoning occurs and catalytic degradation is observed, radical probes are cleaned and a new magnetron sputter coat is deposited.

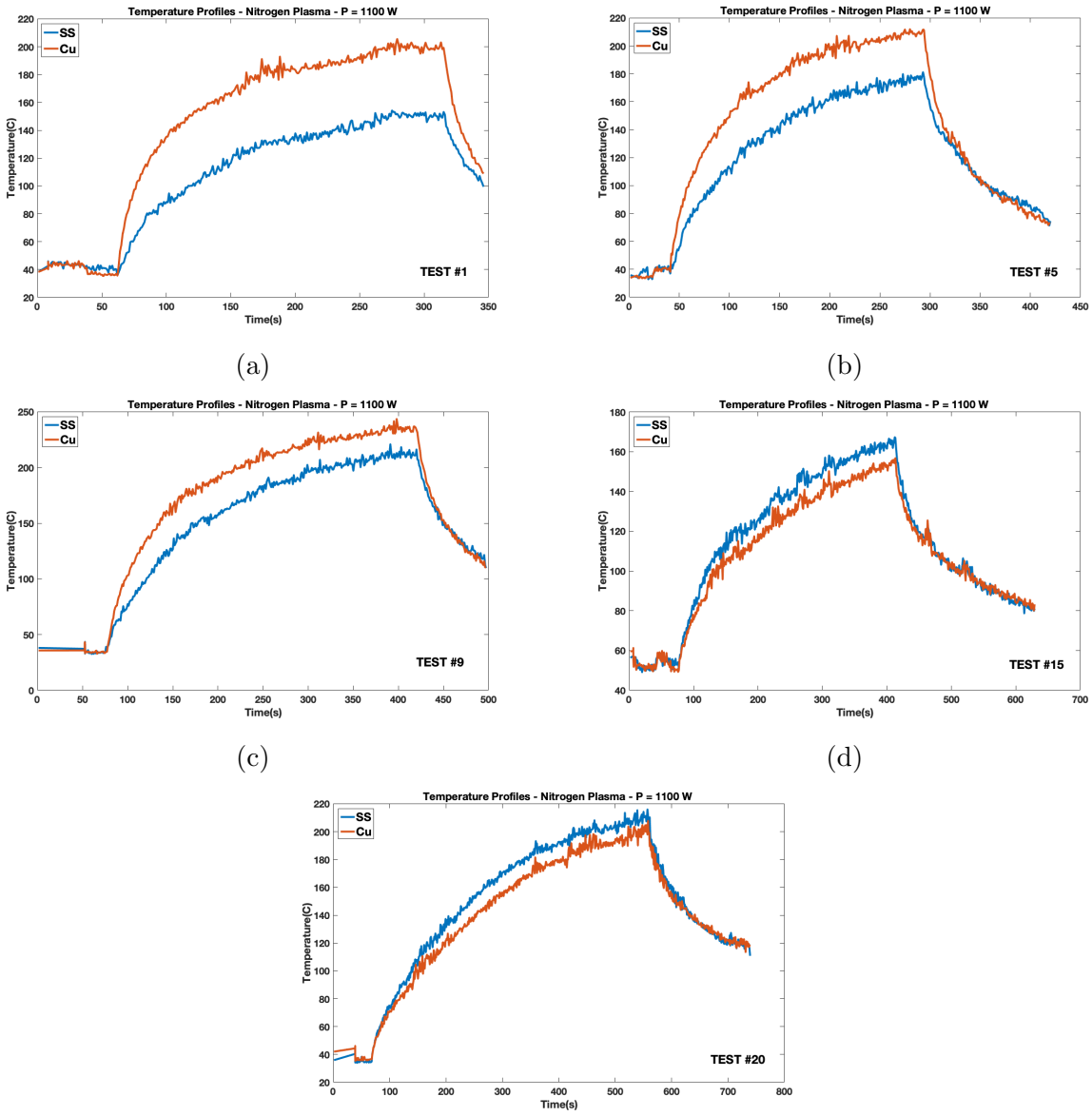

Figure 4.2: Degradation of catalytic properties of radical probe due to changes on surface morphology and formation of oxide/nitride layers on top of the coatings resulting in decrease of sensitivity.

4.1 Hydrogen, Oxygen and Nitrogen

Hydrogen molecules can recombine in various ways, but at low pressures, surface recombination is dominant such that radiative recombination and three-body collision are neglected due to low probability of occurring [2]. Thus, gold surface chemisorbs hydrogen radicals and express high catalytic activity [18]. Hydrogen plasma is characterized at ten pressure points ranging from 10mT up to 100mT by a 10mT increment with RF power varying from 300W to 1100W by a 200W increment. Helicon antenna is automatically matched and only a few watts are reflected back while the forward power is kept constant at a set power. Radical probes and Langmuir probe are placed 30 cm below helicon source bell jar. **Figure 4.3** shows five subplots where the power is constant and pressure changes. Electrons generated in helicon plasma discharge are usually less then 10eV in energy, therefore, dominating collisions between electron and hydrogen molecules are inelastic collisions which leads to dissociation of the molecules, thus generating radicals [18]. Electron temperature decreases as pressure increases since cooling frequency inside plasma chamber increases which in turn decreases electron energy [35]. Also, increased pressure has an inverse relationship with electron collision frequency due to decrease of mean-free-path which results in electrons losing their energy and momentum [34]. Reiterating that electron temperature is determined by the slope of natural logarithm of electron current between plasma and floating potential in IV trace [11]. Similar drop of electron temperature with increase of pressure can be seen [36] [37] Also, it is observed that electron temperature increases slightly with the rise of power, going from about 1eV at 100mT and 300W to about 10eV at 10mT at 1100W, see **figures 4.3.a** and **4.3.e** respectively. Additionally, **figure 4.4.c** shows electron temperature behavior with increase of power such that it is observed that in higher power regimes it's easier to see the increase of temperature.

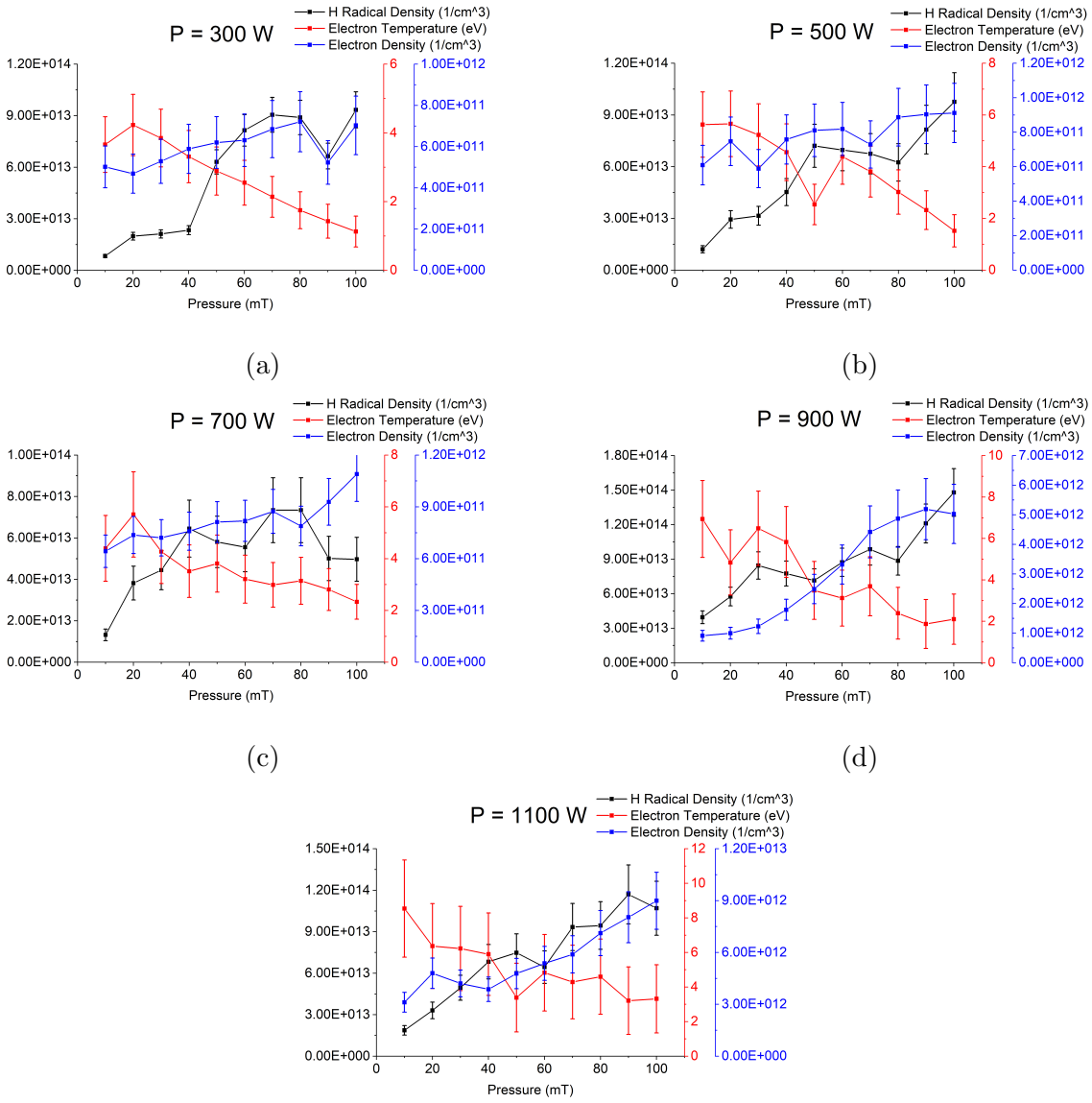

Figure 4.3: Hydrogen radical density, electron density and electron temperature with varying pressure and power.

Electron density has an inverse relationship compared to electron temperature, it goes up as pressure increases, this behavior can be observed clearly in higher power regimes such as 900W and 1100W. Densities vary from $10^{11}/cm^3$ at 10mT and 300W up to $9 * 10^{12}/cm^3$ at 100mT at 1100W, such can be seen at **figures 4.3.a** and **4.3.b**, respectively. Also, **figure 4.4.b** shows increase of electron density as power increases. Electron density measurements

depend on expansion of the sheath around the Langmuir probe and the collision processes which occur in the sheath [38]. On other hand, hydrogen radical density has similar behavior as electron density with respect to pressure and power, however, hydrogen radical density is greater by up to two orders of magnitude then electron density for the same experimental conditions. Although, in **figure 4.4.a** increase of power does not yield significant density increase, nevertheless, upward density behavior is observed.

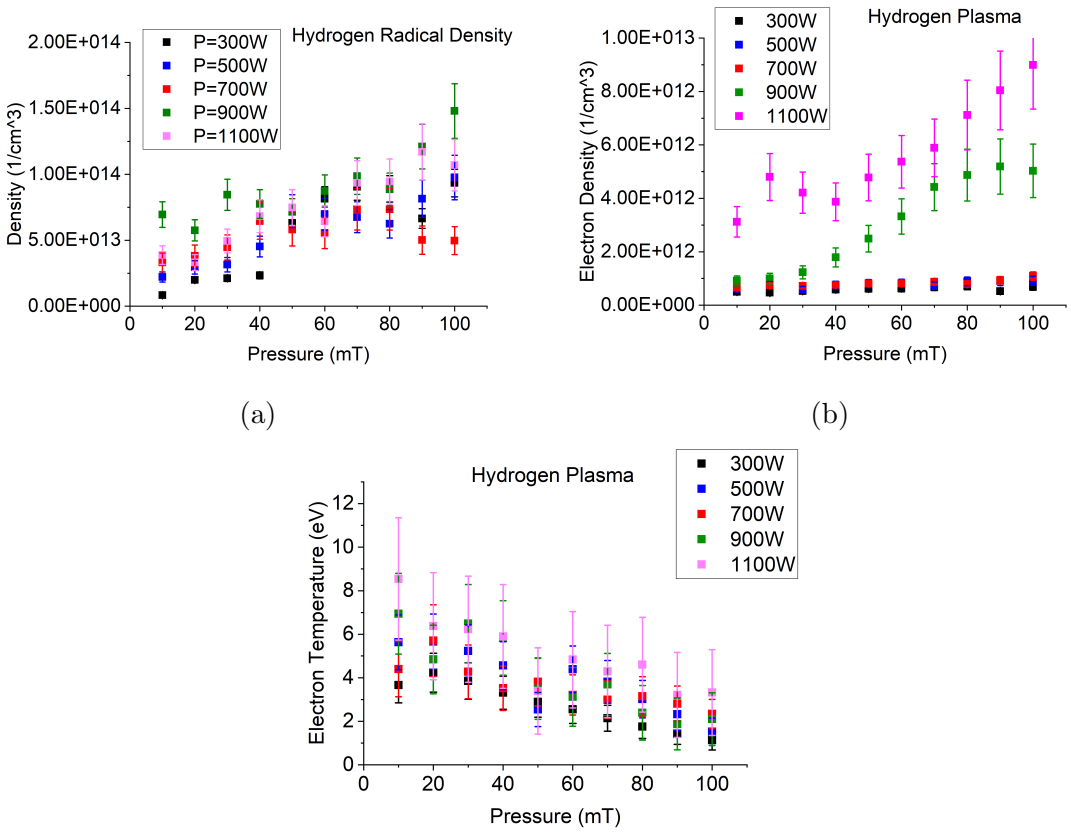

Figure 4.4: Hydrogen plasma diagnostics parameters with varying pressure and power.

Figure 4.4 shows a summary of results for hydrogen gas. Overall, electron temperature, electron density and radical density increase with increase of RF power, specifically electron density. All measurements are taken when probes (LP and RP) are mounted in the center ($r = 0\,cm$) of the HARP chamber, we expect all measured plasma parameters to decreases as radius increases [8].

Results for oxygen and nitrogen gases exhibit similar patterns with respect to plasma parameters. Measurement method is the same for all three gases individually. Electron density and oxygen radical density increases with pressure and power as it is expected whereas electron temperature for oxygen plasma decreases with pressure and increases with power, see **figure 4.6**. Radical density in plasma environment depends also on size and shape of chamber since a high percentage of recombinations happen on the walls [31]. Similarly to hydrogen plasma, oxygen radical density changes more as pressure increases compared to power changes. Also, oxygen radical density and electron density are higher then hydrogen densities but comparable to nitrogen densities due to higher ionization cross-section and ionization efficiency [39] which is also shown in the following section 4.2. Electron density for oxygen plasma varies from $2 * 10^{11}/cm^3$ at 10mT and 300W up to $9 * 10^{12}/cm^3$ at 100mT and 1100W see **figure 4.6.b**. In low pressure regimes, electron density of oxygen plasma is not much noticeable. Electron temperature in oxygen plasma varies from 0.5eV at 300W and 80mT up to a maximum value of 9.2eV at 10mT and 1100W which can be seen in **figures 4.5.a** and **4.5.e**. Probe temperatures are generally lower with hydrogen plasma compared to oxygen and nitrogen as well [5]. However, at higher pressures electron temperature is less distinguishable with varying power.

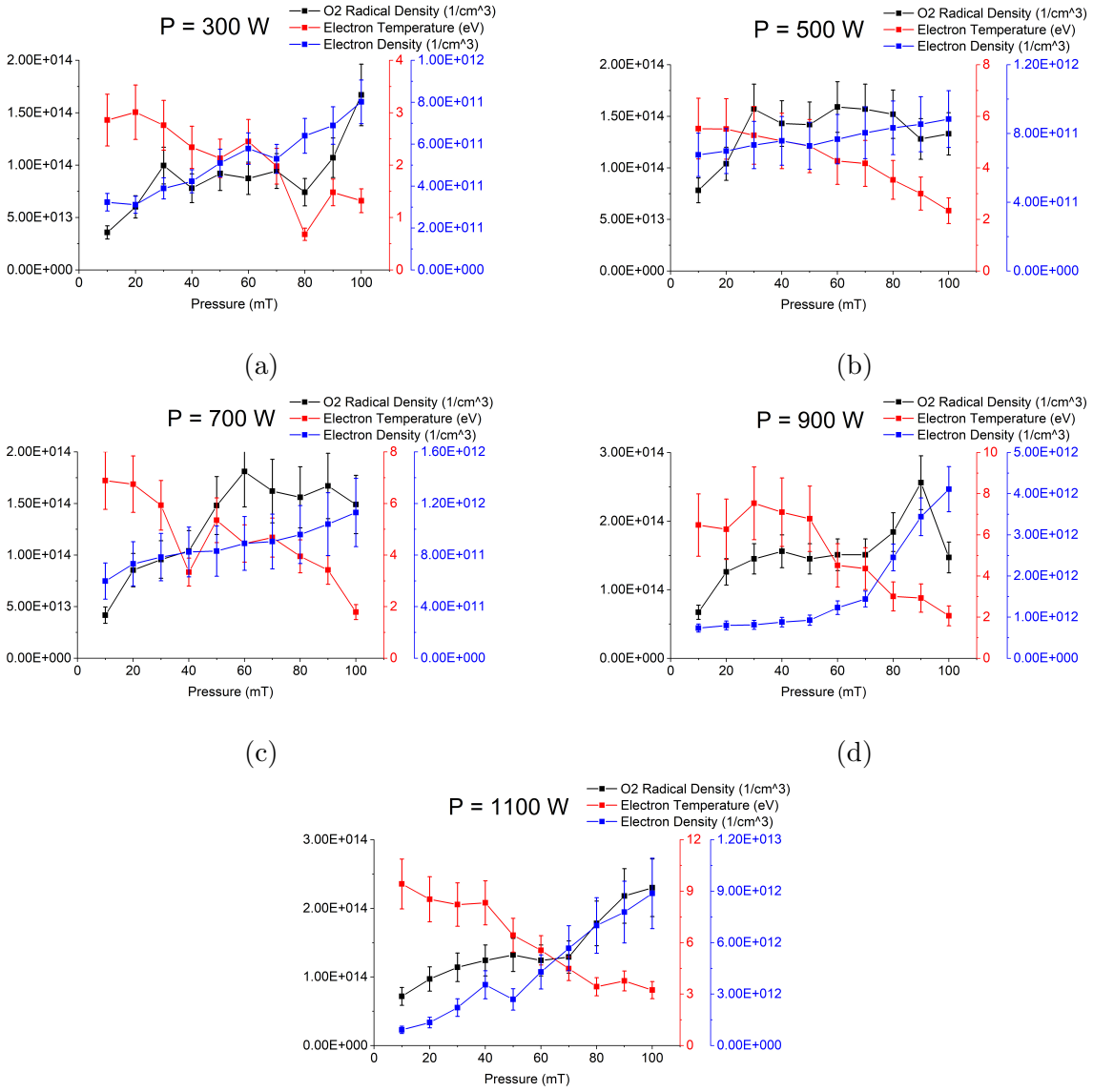

Figure 4.5: Oxygen radical density, electron density and electron temperature with varying pressure and power.

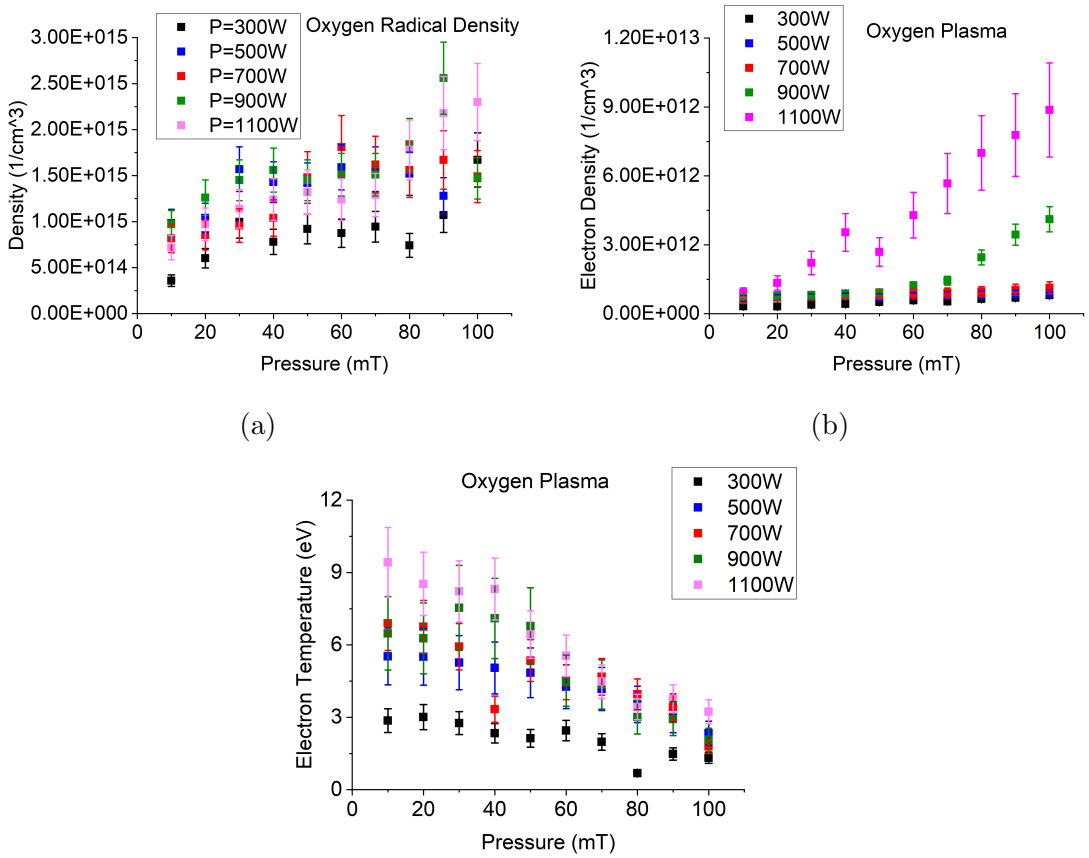

Figure 4.6: Oxygen plasma diagnostics parameters with varying pressure and power.

Nitrogen plasma measurements follow the expected behavior very similarly to hydrogen and oxygen plasmas. Electron density and temperature is comparable to oxygen but nitrogen radical density is slightly lower than oxygen radical density. Electron density for nitrogen plasma varies from $2 * 10^{11}/cm^3$ at 10mT and 300W up to about $7 * 10^{12}/cm^3$ for 100mT at 1100W and electron temperature varies from 2 eV up to 10 eV over the measurement intervals.

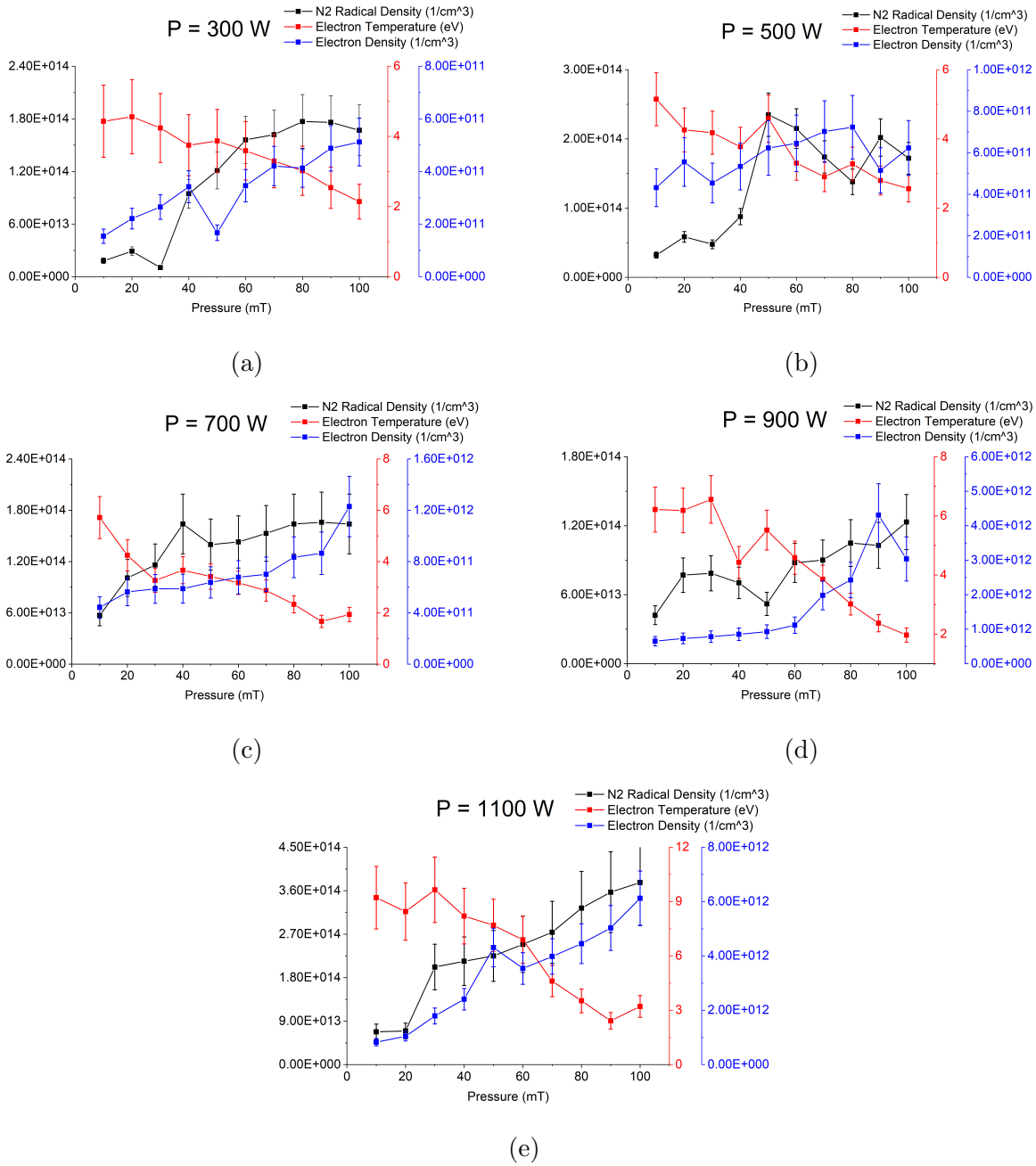

Figure 4.7: Nitrogen radical density, electron density and electron temperature with varying pressure and power.

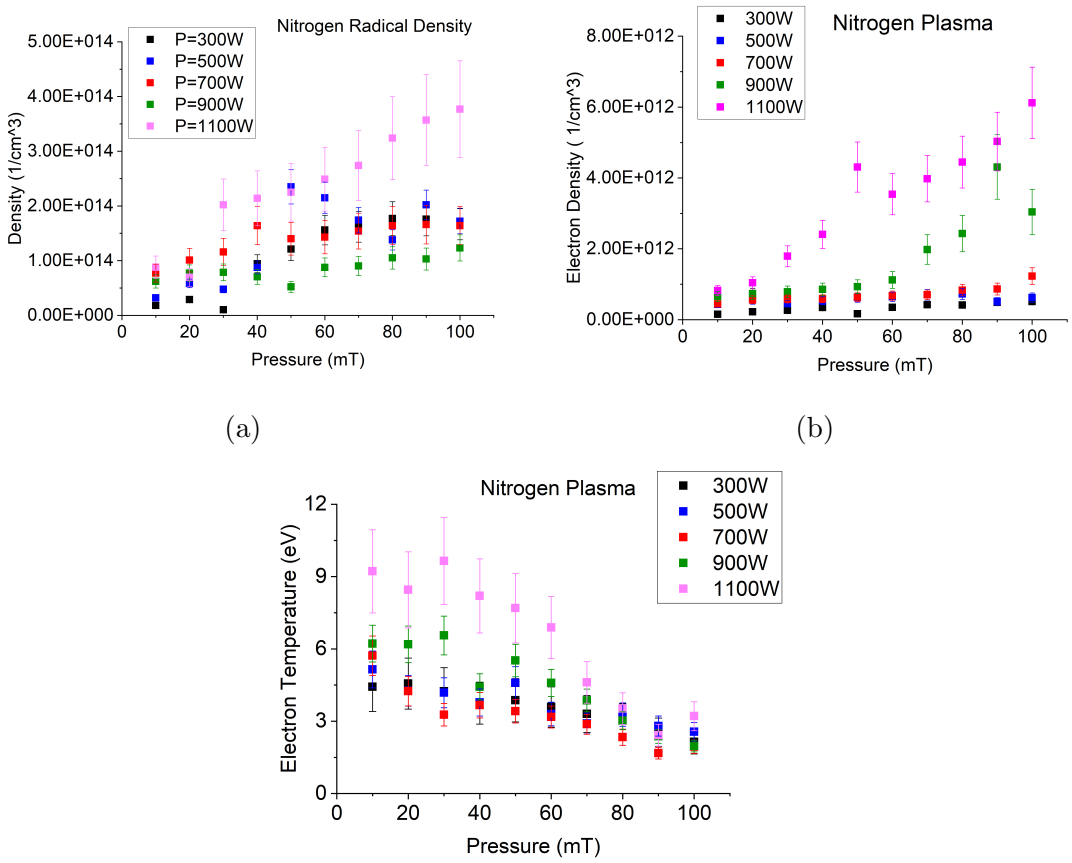

Figure 4.8: Nitrogen plasma diagnostics parameters with varying pressure and power.

All three gases measured separately acted similarly under same experimental conditions. Radical density and electron density of oxygen and nitrogen are higher then for hydrogen but electron temperature does not vary significantly amongst gases. Main source of error in radical density measurement is recombination coefficient due to its dependency on many factors as shown by [31] [40] [41]. This error is smaller when a single gas is present in the chamber [42] [19].

4.2 Mixed Gases

Radical probe system is capable of working with a mixture of gases present in HARP chamber. Probe array can be build as such to detect radical density of many gases. **Figure 3.4** show an array system with six probes, five of which are coated with different catalytic material and one is bare stainless-steel such that temperatures can be differentiated from it. However, radical probe system theoretically can be designed for unlimited number of probes. **Figure 4.9.a** shows the study case when helium, nitrogen and hydrogen gases are by a three-probe system. Initially, when plasma is turned on at 300W and 70mT, only 25 standard cubic centimeter per minute (sccm) of helium gas is supplied. During this interval the temperature of the probes are relatively the same because helium gas is inert gas therefore does not activate catalytic processes. At time interval of 640 seconds, flowrate of hydrogen and nitrogen is increased at 5 sccm while helium flowrate is decreased at 5 sccm such that total pressure is maintained at 70mT. Here, we observe difference of temperatures, where temperature of copper and gold coated probes increase significantly since copper surface has high recombination coefficient for nitrogen radicals and gold surface has high recombination coefficient for hydrogen radicals. Once the plasma is off, it is observed that temperatures converge at a lower point. **Figure 4.9.b** shows temperature profiles gold and stainless-steel probes when exposed to a gas mixture of helium and hydrogen only at a pressure of 50mT and power of 500W. When only helium gas is flowing at 25 sccm, temperature difference is relatively small, however, once hydrogen is introduced into the chamber with a 6 sccm flowrate and helium's flowrate is dropped at 10 sccm such that pressure is kept constant, it is observed significant temperature difference between the probes due to effect of recombination coefficient of hydrogen on gold surface.

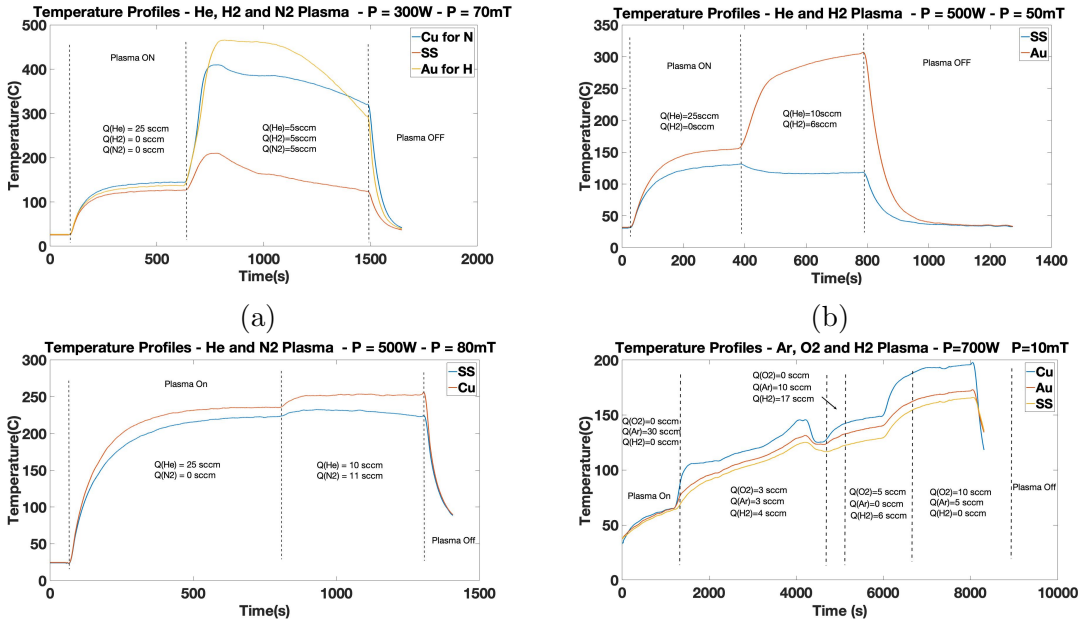

Figure 4.9: Sensitivity of probe when mixed gases are present.

Figure 4.9.c shows the temperature measurements of copper and stainless-steel probes when exposed to helium and nitrogen gas. The experimental procedure is follows same procedure as previous cases. Initially, helium is flown at 25 sccm at 500W and 80mT. Then flowrates are changed accordingly by increasing nitrogen at 11 sccm and decreasing helium at 10 sccm such that temperature difference increases in the right side of the graph due to recombination of nitrogen radicals on copper surface. **Figure 4.9.d** represents the case when argon is used as inert gas together with oxygen and hydrogen to test three-probe system with copper and gold as catalytic material. When plasma is turned on, only 30 sccm of argon flows and temperature of three probes is the same. In the second interval at 1200 seconds onset, flowrates of argon, oxygen and hydrogen are 3 sccm, 3 sccm and 4 sccm, respectively. During second interval copper and gold probe temperatures increase due to recombination of oxygen radicals on copper catalytic surface and hydrogen on gold catalytic surface. In the third interval, it is observed that copper probe temperature decreases due to stop of oxygen flowrate, which shows good response of probe sensitivity. In the forth time interval at 4600 seconds onset, temperature profiles of copper and gold probes increases more due to absence

of argon in the chamber. In the last time interval, hydrogen flowrate is zero whereas oxygen flowrate is 10 sccm and argon flowrate is 5 sccm such that significant increase of copper probe temperature is observed. **Figure 4.9** shows probe system can clearly differentiate between gases in terms of radical measurements when proper gas to catalytic material pair is chosen.

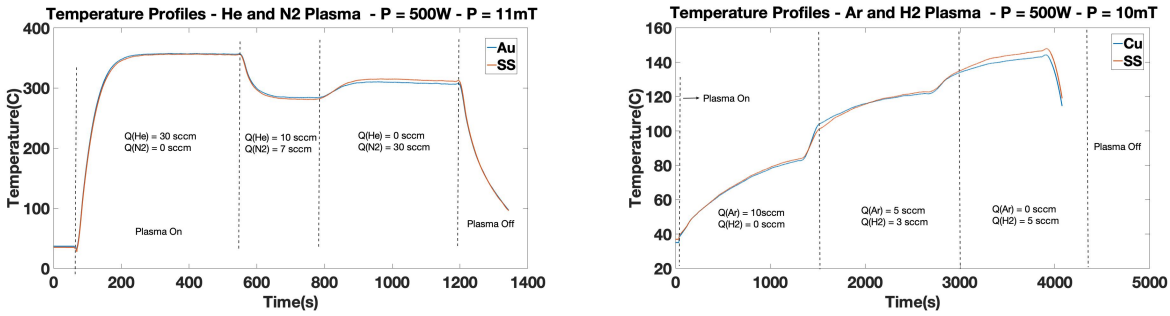

(a) (b)

Figure 4.10: Non-sensitivity of catalytic material to certain gases.

Figure 4.10 shows the opposite of **figure 4.9**. Here, gas to catalytic material pair is purposefully chosen such that recombination coefficients are small therefore no temperature differences can be observed. **Figure 4.10.a** shows temperature profiles for gold and stainless-steel probes when exposed to helium and nitrogen gas at 11mT and 500W. The graphs is split in three interval with combinations of nitrogen and helium gas flowing and only overall temperature changes but not for individual probes. Also, in **figure 4.10.b**, copper and stainless-steel probes are exposed to argon and hydrogen plasma at 10mT and 500W. Again, similarly in all three intervals with argon and hydrogen flow combinations, only overall temperature of the chamber increases but there is no temperature deference between probes. This occurs because hydrogen does not activate copper as catalytic material and nitrogen does not activate gold as catalytic material therefore their respective recombination coefficients are very small [43].

A comparison of all three gases shows their ionization and radical density percentages follows the behavior of total ionization cross-sections. Ionization percentage is found by dividing electron density to overall gas density in the chamber in the following fashion.

Initially, total gas density of the chamber is determined by equation 4.1:

$$n_{tot} = \frac{p}{k_B T} \tag{4.1}$$

For a study case for hydrogen plasma where P =30mT and P =900W , p is given in Pascal, temperature is in Kelvin such that $P = 30mT = 3.9996Pa$ and $T = 260C = 533.15K$. Therefore, total gas density is:

$$n_{tot} = \frac{3.9996Pa}{1.38 \times 10^{-23} \frac{m^2 kg}{s^2 K} \times 533.15K} = \frac{5.44 \times 10^{14}}{cm^3} \tag{4.2}$$

Next, in order to find ionization percentage and radical density percentage, electron density and radical density at the given experimental conditions are divided by total gas density, $n_H = 8.45 \times 10^{13}/cm^3$ and $n_e = 1.23 \times 10^{12}/cm^3$, respectively. Note, error bars are determined via same procedure as in section 2.1, equation 2.11.

$$Ionization(\%) = 100 \times \frac{n_e}{n_{tot}} = \frac{1.23 \times 10^{12}/cm^3}{5.44 \times 10^{14}/cm^3} = 0.0226 \tag{4.3}$$

$$RadicalDensity(\%) = 100 \times \frac{n_H}{n_{tot}} = \frac{8.45 \times 10^{13}/cm^3}{5.44 \times 10^{14}/cm^3} = 15.53 \tag{4.4}$$

Figure 4.11.a shows ionization percentage as function of power. The values are averaged for pressure range between 10mT and 100mT since we did not observe any change with respect to pressure. As power increases, ionization percentage increases as well however it is noticed that ionization percentage for oxygen and nitrogen is quite similar and higher then hydrogen. This phenomenon occurs because total ionization cross-section for oxygen and nitrogen is similar and also higher than hydrogen as seen in the **figure 4.12**. Therefore, same amount of given power generates smaller ionization efficiency for hydrogen.

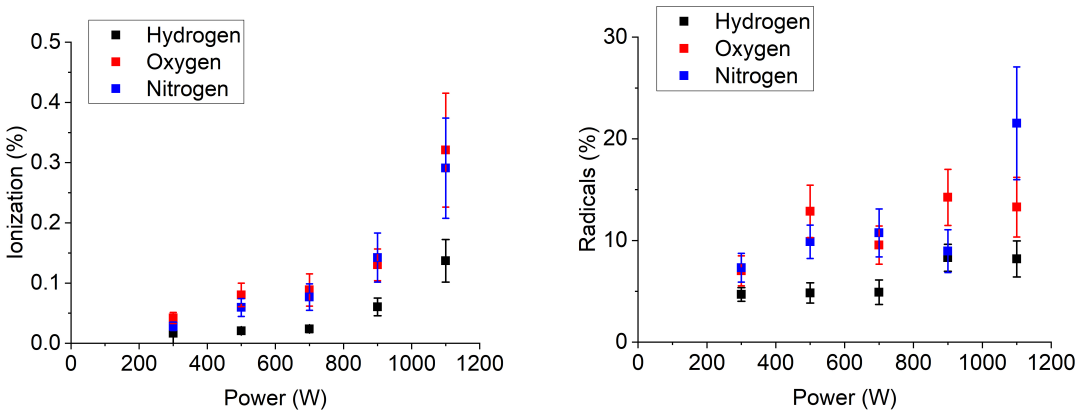

(a) Ionization percentage of all gases (b) Radical density percentage of all gases

Figure 4.11: Ionization and radical density percentages for all three gases

Similarly, radical density percentage, which is found by dividing radical density to overall gas density in the chamber, follows similar pattern with ionization percentage although values are much higher. At higher powers, radical density percentage increases. Here too, oxygen and nitrogen radical density percentage is higher than hydrogen because the main generative mechanism of radicals in low pressure regimes is via electron dissociation [30]. Therefore, the more electrons generated at higher ionization efficiency more radicals are created as consequence.

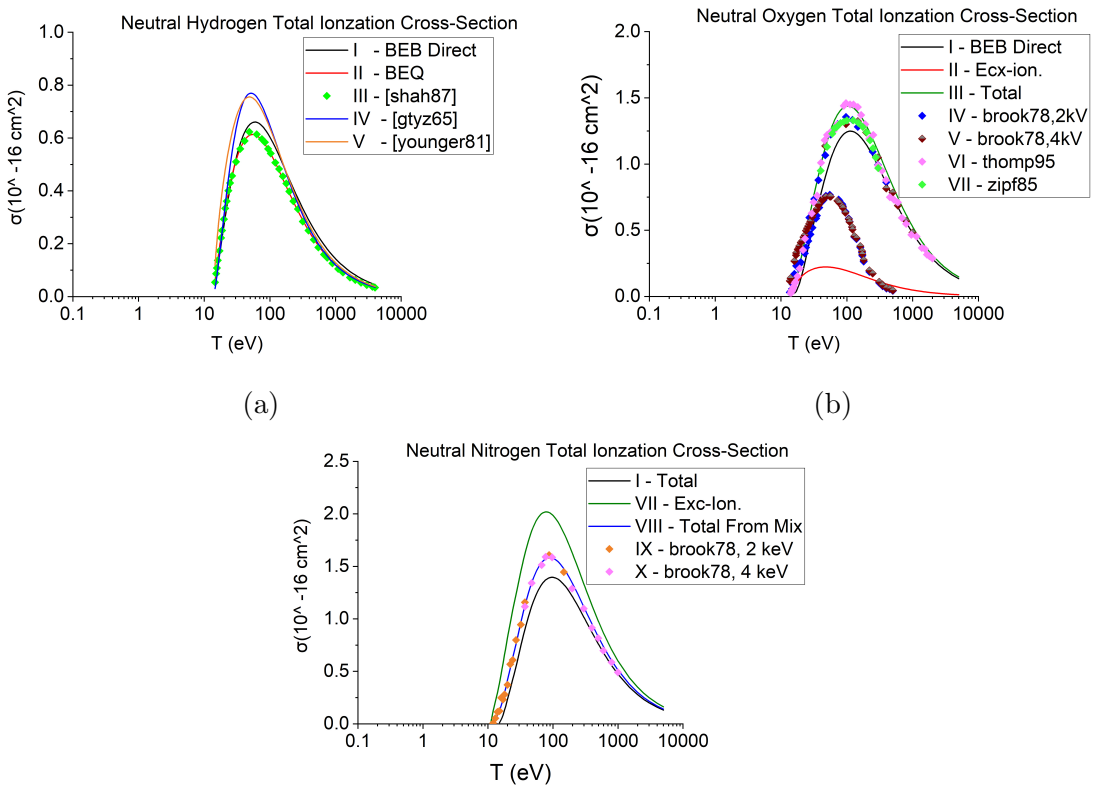

Figure 4.12: Total Ionization Cross-Sections for Hydrogen, Oxygen and Nitrogen

Chapter 5

Conclusions and Future Work

The ever increasing demand for more control and deeper understanding over atom-scale processes leads to development of new in-situ tools which are reliable and adaptable. Specifically, semiconductor industry is the leading promoter of such developments due to its very nature. Knowing concentration of species inside vacuum systems helps us better understand their effects and role they play in physical and chemical processes. Further comprehension of physical processes and their consequences help to develop science to reach new realms and also help to develop new cutting edge technology which ultimately increases quality of our lives and makes them better.

In this study, an in-situ radical probe system is developed together with the Ra-Den software at Center for Plasma and Material Interactions (CPMI). Radical probe system has high spatial resolution and it is a tool which is easily modified and it can be adapted in numerous plasma processing vacuum chambers. Compared to optical emission spectroscopy (OES) tools, radical probe system is inexpensive and easy to be built. This system can be used for industrial and research purposes. Main advantages are the ability to measure densities in steady state plasma conditions and ability to operated in a mixture of gases environment.

Radical densities of hydrogen, nitrogen and oxygen were measured in HARP helicon chamber by sweeping power from 300W up to 1100W and by sweeping pressure from 10mT up to 100mT. Generally, it is observed that radical densities increase with respect to pressure and power, accordingly. Additionally, plasma is parametrized by electron density and electron temperature such that electron density increased with increasing power and pressure and

electron temperature increased with increasing power but it did decrease with increasing pressure. Further tests showed that radical probe system is capable of detecting specific gases when a mixture of gases is present in the chamber based on known recombination coefficient of the given gas on catalytic surface. Ionization and radical density percentages of all three gases are compared to total ionization cross-sections of each gas, agreement is observed for each corresponding gas.

In terms of the future work, higher credibility of measured radical densities could be achieved by comparing the values of OES measurements in the same vacuum system and under the same experimental conditions. Measuring radical concentration via different measurement methods will give more credibility to our obtained values, specially combining non-invasive methods with invasive methods. The biggest issue regarding this study is related to recombination coefficient values due to their dependence on variety of factors and due to this fact it is quite difficult for academia to agree on specific values because every experimental design and methodology is different. Mechanisms of recombination coefficient of gases on surfaces are yet to be fully understood quantitatively. Varying parameters such pressure, temperature, coating thickness, impurities on the surface and chamber size affect physics and chemistry of recombining mechanisms. Additionally, recombination coefficient depends of plasma source thus depending on ion concentration present during recombination, specifically ion bombardment onto the surface. Additional research and further understanding is needed in methods of determining recombination coefficient. Also, poisoning of catalytic material due to plasma exposure and impurities plays an important factor of radical probe lifetime. Placing the probes outside plasma radius will prolong the occurrence of contamination and radical detection will still be available. A different potential idea is to manufacture probe made out from catalytic material needed or have the exposed junction of thermocouple made out of catalytic material, this way one can bias at a higher voltage for a longer time which ensures etching of the contamination. Ultimately, contamination of the catalytic surface is inherent and unavoidable.

Furthermore, radical density model based on rate equations will be developed as an auxiliary evidence to support experimental data. Electron energy distribution functions (EEDF) calculated from Langmuir probe data will help build radical density plasma model, this will also help to determine whether Druyvesteyn or Maxwellian distribution function fits better in low pressure plasma regimes. Finally, radical probe system is a promising technology which could be commercialized for wide spread use.

References

[1] M Mozetič, M Kveder, M Drobnič, A Paulin, and A Zalar. Determination of atomic hydrogen density with catalytic probes. *Vacuum*, 45(10-11):1095–1097, 1994.

[2] Miran Mozetic, Alenka Vesel, A Drenik, I Poberaj, and D Babic. Catalytic probes for measuring h distribution in remote parts of hydrogen plasma reactors. *Journal of Nuclear Materials - J NUCL MATER*, 363:1457–1460, 06 2007.

[3] Seiya Yonemori and Ryo Ono. Flux of oh and o radicals onto a surface by an atmospheric-pressure helium plasma jet measured by laser-induced fluorescence. *Journal of Physics D: Applied Physics*, 47:125401, 03 2014.

[4] S Mazouffre, I Bakker, P Vankan, Richard Engeln, and Daan Schram. Two-photon laser induced fluorescence spectroscopy performed on free nitrogen plasma jets. *Plasma Sources Science and Technology*, 11:439, 10 2002.

[5] Joydeep Guha, Rohit Khare, Luc Stafford, Vincent M. Donnelly, Stephen Sirard, and Eric A. Hudson. Effect of cu contamination on recombination of o atoms on a plasma-oxidized silicon surface. *Journal of Applied Physics*, 105(11):113309, 2009.

[6] Miran Mozetic, Alenka Vesel, Virginie Monna, and Alain Ricard. H density in a hydrogen plasma post-glow reactor. *Vacuum*, 71:201–205, 05 2003.

[7] Jake Mclain, Priya Raman, Dhruval Patel, Randall Spreadbury, Jan Uhlig, Ivan Shchelkanov, and D.N. Ruzic. Linear magnetron hipims high deposition rate magnet pack. *Vacuum*, 155, 06 2018.

[8] Francis F Chen. Helicon discharges and sources: a review. *Plasma Sources Science and Technology*, 24(1):014001, jan 2015.

[9] Francis F. Chen. Experiments on helicon plasma sources. *Journal of Vacuum Science & Technology A*, 10(4):1389–1401, 1992.

[10] Martin J. Neumann. Investigation of plasma processing of polymers for use in biomedical applications. 2004.

[11] D.N. Ruzic, W. Weed, and American Vacuum Society. *Electric Probes for Low Temperature Plasmas*. AVS monograph series. American Vacuum Society, 1994.

[12] J. A. (eds.) Paisner, L. J. Radziemski, and R. W. Solarz. *Laser spectroscopy and its applications*. Marcel Dekker, Inc., 1987.

[13] P.A.C. van Zon. Talif measurements on ground state atomic hydrogen behaviour under magnetization. 2013.

[14] J H. Tung, A Z. Tang, Gregory Salamo, and Franky Chan. Two-photon absorption of atomic hydrogen from two light beams. *JOSA B*, 3:837–848, 06 1986.

[15] H.L. Marcus. Auger electron spectroscopy. In K.H. Jrgen Buschow, Robert W. Cahn, Merton C. Flemings, Bernhard Ilschner, Edward J. Kramer, Subhash Mahajan, and Patrick Veyssire, editors, *Encyclopedia of Materials: Science and Technology*, pages 393 – 398. Elsevier, Oxford, 2001.

[16] F BRECELJ, Miran Mozetic, Klementina Zupan, and Matija Drobnic. Behavior of catalytic probes at low pressure. *Vacuum*, 44:459–460, 05 1993.

[17] Aleksander Drenik, Alenka Vesel, Arkadi Kreter, and Miran Mozetic. Recombination of hydrogen atoms on fine-grain graphite. *Applied Surface Science*, 257:5820–5825, 04 2011.

[18] Miran Mozetic, Matija Drobnic, and Anton Zalar. Recombination of neutral hydrogen atoms on aisi 304 stainless steel surface. *Applied Surface Science*, s 144145:399403, 04 1999.

[19] Iztok Sorli and Rudolf Rocak. Determination of atomic oxygen density with a nickel catalytic probe. *Journal of Vacuum Science Technology A: Vacuum, Surfaces, and Films*, 18:338 – 342, 04 2000.

[20] Harmeet Singh, J. W. Coburn, and David B. Graves. Recombination coefficients of o and n radicals on stainless steel. *Journal of Applied Physics*, 88(6):3748–3755, 2000.

[21] K. E. Shuler and K. J. Laidler. The kinetics of heterogeneous atom and radical reactions. i. the recombination of hydrogen atoms on surfaces. *The Journal of Chemical Physics*, 17(12):1212–1217, 1949.

[22] F. Paneth, K. Herzfeld, and F. Paneth. ber freies methyl und freies athyl. *Zeitschrift fr Elektrochemie und angewandte physikalische Chemie*, 37(89):577–582, 1931.

[23] U. Cvelbar, M. Mozeti, I. Poberaj, D. Babi, and A. Ricard. Characterization of hydrogen plasma with a fiber optics catalytic probe. *Thin Solid Films*, 475(1):12 – 16, 2005. Asian-European International Conference on Plasma Surface Engineering 2003 Proceedings of the 4th Asian-European International Conference on Plasma Surface Engineering.

[24] Changyoul Lee, Klaus Luther, Kawon Oum, and Jrgen Troe. Pressure and temperature dependence of the recombination of p-fluorobenzyl radicals. *The Journal of Physical Chemistry A*, 110(8):2613–2621, 2006. PMID: 16494370.

[25] G. A. Hebner. Spatially resolved, excited state densities and neutral and ion temperatures in inductively coupled argon plasmas. *Journal of Applied Physics*, 80(5):2624–2636, 1996.

[26] (Jin-Gor Chang). Deuterium recombination on surfaces of stainless steel and gold. *Chinese Journal of Physics*, 24(3):145–156, Oct 1986.

[27] M.A. Lieberman and A.J. Lichtenberg. *Principles of Plasma Discharges and Materials Processing*. Wiley, 2005.

[28] Robert L. Merlino. Understanding langmuir probe current-voltage characteristics. *American Journal of Physics*, 75(12):1078–1085, 2007.

[29] Francis F. Chen and Jane P. Chang. *Langmuir Probes*, pages 79–93. Springer US, Boston, MA, 2003.

[30] Gerald A. Melin and Robert Madix. Energy accommodation during oxygen atom recombination on metal surfaces. *Transactions of The Faraday Society*, 67, 01 1971.

[31] Miran Mozeti and Anton Zalar. Recombination of neutral oxygen atoms on stainless steel surface. *Applied Surface Science*, 158(3):263 – 267, 2000.

[32] Timmy Cheung, Ferry Schrijer, and Gisu Park. Nitrogen catalytic recombination on copper oxide in tertiary gas mixtures. *Journal of Spacecraft and Rockets*, 53:1–10, 06 2016.

[33] Alenka Vesel. Heterogeneous surface recombination of neutral nitrogen atoms. *Materiali in Tehnologije*, 46:7–12, 01 2012.

[34] Muhammad Yasin Naz, Shazia Shukrullah, Shaharin Anwar Sulaiman, Najeeb ur Rehman, Yasin Khan, Abdul Ghaffar, and Sami Ullah. Investigations on spatial distribution of low temperature plasma parameters using nicr wire probe diagnostic. *Measurement*, 91:194 – 200, 2016.

[35] L. H. Brace, W. R. Hoegy, and R. F. Theis. Solar euv measurements at venus based on photoelectron emission from the pioneer venus langmuir probe. *Journal of Geophysical Research: Space Physics*, 93(A7):7282–7296, 1988.

[36] T Lafleur, C Charles, and R W Boswell. Electron temperature characterization and power balance in a low magnetic field helicon mode. *Journal of Physics D: Applied Physics*, 44(18):185204, apr 2011.

[37] D Gahan, B Dolinaj, and M B Hopkins. Comparison of plasma parameters determined with a langmuir probe and with a retarding field energy analyzer. *Plasma Sources Science and Technology*, 17(3):035026, jul 2008.

[38] J Jauberteau and Isabelle Jauberteau. Determination of the electron density in plasma by means of a floating double probe. *The Review of scientific instruments*, 79:033505, 04 2008.

[39] Z. Kregar, R. Zaplotnik, M. Mozeti, and S. Miloevi. Comparison of spatial distributions of atomic oxygen and hydrogen in icp by means of catalytic probes and actinometry. *Vacuum*, 109:8 – 14, 2014.

[40] Shunji Takahashi, Seigo Takashima, Koji Yamakawa, Shoji Den, Hiroyuki Kano, Keigo Takeda, and Masaru Hori. Development of atomic radical monitoring probe and its application to spatial distribution measurements of h and o atomic radical densities in radical-based plasma processing. *Journal of Applied Physics*, 106:053306 – 053306, 10 2009.

[41] P. G. Dickens and M. B. Sutcliffe. Recombination of oxygen atoms on oxide surfaces. part 1.activation energies of recombination. *Trans. Faraday Soc.*, 60:1272–1285, 1964.

[42] M. Mozetic, A. Vesel, A. Drenik, I. Poberaj, and D. Babic. Catalytic probes for measuring h distribution in remote parts of hydrogen plasma reactors. *Journal of Nuclear Materials*, 363-365:1457 – 1460, 2007. Plasma-Surface Interactions-17.

[43] J. C. Greaves and J. W. Linnett. Recombination of atoms at surfaces. part 4theory of method and mesurement of atom concentrations. *Trans. Faraday Soc.*, 55:1338–1345, 1959.

[44] M Mozeti, M Drobni, A Pregelj, and K Zupan. Determination of density of hydrogen atoms in the ground state. *Vacuum*, 47(6):943 – 945, 1996. Proceedings of the 13th International Vacuum Congress and the 9th International Conference on Solid Surfaces.

[45] Daniel Tyler Elg, Gianluca A. Panici, Jason A. Peck, Shailendra N. Srivastava, and David Neil Ruzic. Modeling and measurement of hydrogen radical densities of in situ plasma-based sn cleaning source. *Journal of Micro/Nanolithography, MEMS, and MOEMS*, 16, 2017.